THESIS

AN OBJECT-BASED ANALYSIS OF LIGHTNING CHARACTERISTICS IN PRE-TROPICAL CYCLOGENESIS ENVIRONMENTS

Submitted by

Nicholas A. Mesa

Department of Atmospheric Science

In partial fulfillment of the requirements

For the Degree of Master of Science

Colorado State University

Fort Collins, Colorado

Summer 2025

Master's Committee:

Advisor: Michael M. Bell

Kristen L. Rasmussen
John van de Lindt

ABSTRACT

AN OBJECT-BASED ANALYSIS OF LIGHTNING CHARACTERISTICS IN PRE-TROPICAL CYCLOGENESIS ENVIRONMENTS

The Geostationary Lightning Mapper (GLM) on GOES-16 provides continuous, high-resolution data that enables a novel investigation of lightning attributes in pre-tropical cyclogenesis environments. An object-based framework, which provides additional spatiotemporal characteristics, was used to evaluate the area and optical energy of GLM lightning groups through the Tracking and Object-Based Analysis of Clouds (tobac) Python package. Applying tobac's compositing and tracking methods to GLM observations was first tested with a case of genesis (Tropical Storm Claudette (2021)) within range of the NEXRAD network. Collocated ground-based, dual-polarization radar observations suggested that small-area and low-energy lightning was indicative of stronger convection and updrafts via composite vertical radar profiles of tobac lightning features. The physical interpretations of these lightning attributes were then applied to lightning 72 hours prior to genesis and within 200 km of the best-track invest center for four developing disturbances (Claudette (2021), Ida (2021), Earl (2022), and Beryl (2024)). The presence of small-area and low-energy lightning, previously associated with stronger updrafts and convection, was seen at various times prior to genesis for all cases. Large-area and high-energy lightning was also identified for all cases at various times in the analysis period. Lightning was suggested to be modulated by deep-layer vertical wind shear, and multiple instances of electrified convection were noted to coincide with improvements in organization. More work is needed to evaluate these lightning attributes in a larger composite of pre-genesis disturbances. This work offers a novel characterization of oceanic lightning in pre-tropical cyclogenesis environments for the North Atlantic basin.

ACKNOWLEDGEMENTS

I would first like to thank my family, whose unconditional love and support have empowered me to be lucky enough to pursue my childhood dreams of studying tropical cyclones. To my Mom and Dad, thank you for everything. Expressing my gratitude for all you have provided me would be longer than the thesis itself. To my younger sister, Katherine, your endless drive and passion for pursuing what you love inspire me to work harder and tap into my own passions every day. I would also like to thank my advisor, Michael Bell, for the opportunity to pursue my graduate education at CSU and for his mentorship, which has guided my entry into the atmospheric sciences. This work could not have been done without the insights of an incredible science team, which included Michael Bell, Benjamin Trabing, Alan Brammer, Phillip Klotzbach, Patrick Duran, Kate Musgrave, and Stephanie Stevenson. Thank you to Jennifer DeHart and Ya-Chien Feng for their code and insights regarding the radar portion of this project. I would also like to acknowledge financial support from the American Meteorological Society Graduate Fellowship and NASA ROSES Award 80NSSC23K1530. To Isaac and Delián, thank you for being my first and best friends during my time in Fort Collins. Words cannot express how much your friendship has impacted my experience for the better here. Thank you as well to all members of the Bell Group, both past and present, for your companionship and mentorship. To the friends, professors, scientists, and staff on The Hill, thank you for making the Department such a special place to work and a joy to come to every day. And finally, to all my teachers, professors, scientists, and mentors over the years, thank you for helping to shape me into the student and aspiring scientist I am today.

DEDICATION

I would like to dedicate this thesis to my Mom, Dad, and sister, as well as the special group of 12 friends from home who have been my roommates, neighbors, best friends, and biggest supporters over the many years.

TABLE OF CONTENTS

LIST OF TABLES

LIST OF FIGURES

Chapter 1

Introduction

Tropical cyclones (TCs) are the costliest weather disasters in the United States, accounting for $1.4 trillion in estimated costs and damages since 1980 (NOAA National Centers for Environmental Information, 2025). The majority of TC impacts are felt in coastal areas that are the most vulnerable to storm surge, freshwater flooding, and high winds. This vulnerability to TC hazards continues to be exacerbated by observed increases in the net migration of people to high hurricane-risk areas, which has dramatically risen since the COVID-19 pandemic (Mac Home, 2022). The National Oceanic and Atmospheric Administration (NOAA) has made it a priority to mitigate impacts from these hazards through the Hurricane Forecast Improvement Project (HFIP; Gall et al. 2013). While HFIP has successfully driven significant improvements in hurricane track and intensity forecasts, NOAA still aims to improve guidance on pre-formation disturbances, including tropical cyclogenesis timing, track, and intensity forecasts, to maximize the lead time of TC impacts (Marks et al., 2019).

Improving guidance related to tropical cyclogenesis (hereafter referred to as genesis) remains a priority due to its inherent difficulty to forecast. The 2024 North Atlantic hurricane season emphasized this difficulty, as the National Hurricane Center (NHC) noted that several genesis events were poorly forecast or not well anticipated (https://www.nhc.noaa.gov/data/tcr/index.php?season=2024&basin=atl); the most notable case being Hurricane Milton, whose genesis was "very poorly forecast" four days before making landfall in Florida, causing over $34 billion in damages (Beven II et al., 2025a). While significant strides have been made in cultivating a better understanding of factors relevant to genesis, particularly within the past two decades, limitations remain. In addition to the reliance of genesis on otherwise stochastic deep convection, fundamental questions remain regarding various internal and external processes across spatial and temporal scales prior to genesis (Tang et al., 2020).

Organized deep convection has long been considered an essential phenomenon for the genesis and intensification of tropical cyclones (e.g., Gray 1968). An important subset of deep convection contributing to genesis is the vortical hot tower, first identified as a primary feature in genesis via numerical studies (Hendricks et al. 2004; Montgomery et al. 2006). VHTs are characterized by strong, rotating updrafts within deep convection with small planar areas compared to their tall, vertical structure. VHTs facilitate the concentration of potential vorticity (PV) in the lower troposphere through high vertical mass flux and the ensuing increase in the gradient of latent heat with height. VHTs later serve to strengthen the mid-level circulation in the mesoscale convective vortex (MCV) as well (Reasor et al. 2005; Houze et al. 2009; Bell and Montgomery 2019). Houze et al. (2009) presented the first direct observation of a VHT in a developing tropical depression and illustrated how strong, rotating updrafts associated with VHTs amplified vorticity at lower levels. Houze et al. (2009)'s results were similar to those of Zipser and Gautier (1978), where the latter identified a strong and broad updraft region resembling a VHT embedded within a mesoscale convective system (MCS). This massive updraft was found to be sufficient for the eventual intensification of the disturbance off the west coast of Africa. VHTs and deep convection, in general, are also known to moisten the overall environment, increasing buoyancy and facilitating the eventual conversion of a disturbance to a tropical cyclone vortex (Nolan, 2007).

Strong updrafts within VHTs and deep convection can often produce lightning. The production of lightning via strong updrafts follows the Non-Inductive Charging mechanism, in which an updraft facilitates the collision of small, upwelling ice crystals and supercooled liquid water with larger and heavier hail and graupel (Takahashi, 1978). These collisions result in a charge separation, with lightning serving as the eventual discharge. Bruning and MacGorman (2013) found that lightning associated with stronger updrafts and convection was associated with more frequent, less energetic, and smaller flashes. That work, which focused on supercells in Oklahoma using very high frequency (VHF) Lightning Mapping Arrays (LMAs), also found that stratiform lightning was characterized by less frequent, more energetic, and broader flashes. Bruning and MacGorman (2013) suggested that these convective and stratiform lightning attributes were products of the

overall cloud structure and dynamics. For example, deep convective cells are concentrated across small planar areas containing strong updrafts, allowing for flashes over a smaller-area charge layer with faster charging rates. On the other hand, stratiform features, which may be characterized by broad spatial extents and weaker updrafts, lend to larger flash areas over broader charge layers and slower charging rates. Relationships between lightning attributes and convective morphology have not been validated for oceanic convection. In general, lightning over the ocean is less common, larger, brighter, and longer in duration compared to land (Rudlosky et al., 2019).

As previously discussed, deep convection and stratiform processes are important in the lead-up to genesis through various dynamic and thermodynamic mechanisms. If lightning attributes are indicative of these convective morphologies, we hypothesize that lightning and its attributes may be relevant in diagnosing convective and stratiform processes in pre-genesis environments. Specifically, we hypothesize that smaller-area, lower-energy lightning (i.e., stronger convection) in the earlier stages of a VHT contributes to low-level vorticity production via vortex stretching. In comparison, larger-area and higher-energy lightning (i.e., weaker convection or stratiform) in the decaying stages of the same VHT may indicate a developing mid-level circulation. Thus, this manuscript seeks to link known lightning attributes associated with the different convective morphologies to evaluate trends in lightning leading up to genesis.

Despite the suggested relationship between deep convection, lightning, and genesis, a limited amount of work has examined lightning prior to genesis. Leary and Ritchie (2009) was one of the first studies to explore the question of lightning and genesis, looking at eastern North Pacific tropical disturbances using land-based detection networks during the 2006 hurricane season. This work found that developing disturbances had a considerably larger quantity of lightning flashes than those that did not. Leppert et al. (2013b) used the spaceborne Lightning Imaging Sensor to come to similar conclusions for the eastern North Pacific basin; however, no statistical differences in lightning flash rates (or other metrics of convective intensity, such as radar reflectivity and microwave imager brightness temperatures from the Tropical Rainfall Measuring Mission) were found for east Atlantic developing and non-developing waves. Leppert et al. (2013a) used the same datasets

in a Lagrangian framework to confirm the lack of significance provided by convective intensity indicators (lightning included). Their work did find, however, that on or near the day of genesis, lightning flash rates were significantly less for developing waves, suggesting less intense convection during genesis. Zawislak and Zipser (2014) also found that estimates of convective intensity did not appear to be a differentiating factor for developing and non-developing disturbances in the North Atlantic, though other convective metrics were suggested as discriminators for developing disturbances. These convective metrics included a maximum areal fraction of strong convection within 3° latitude/longitude of the storm center between 1 and 2 days prior to genesis, in addition to a greater fraction of strong and intense convective events. Additionally, it was suggested that early and "favorable" convective processes may not be directly responsible for formation but aid in the beneficial modification of the environment. Wang (2018) agreed that convective intensity was not a key feature for genesis in their "pouch-oriented" approach, but they did find a trend of intensifying convection near the pouch center. This difference was suggested to be the result of using a smaller domain in their quasi-Lagrangian, wave pouch-centric framework, which utilized geostationary infrared (IR) brightness temperature data from multiple geostationary satellites in the GridSAT-B1 dataset. The successful use of geostationary satellite data in this smaller, quasi-Lagrangian domain to evaluate trends in developing versus non-developing disturbances suggests that more research is needed to better utilize geostationary satellite-based analyses for genesis. The new Geostationary Lightning Mapper (GLM) presents a particularly intriguing opportunity, given the novelty of the continuous, high-resolution, spaceborne lightning data it provides in comparison to previous work.

The launch of GOES-16 in 2016 marked the introduction of GLM, the first lightning mapper in geostationary orbit (Goodman et al. 2013; Rudlosky et al. 2019). Previous studies that used land-based mappers were limited by their instruments, with detection efficiency tapering off with increased distance from the coast. Past iterations of spaceborne lightning sensors, such as the Lightning Imaging Sensor, were in inclined orbits and only provided a brief snapshot of observed lightning if the sensor passed over the area of interest. GLM improved upon these limitations by

continuously observing lightning across an entire hemisphere with high detection efficiency (e.g., Bateman and Mach 2020; Bateman et al. 2021). Furthermore, GLM enabled the characterization of lightning beyond flash quantity and rate, which were typically used in prior work. Specifically, area and energy attributes from GLM provided insight into convective and stratiform processes in tropical disturbances of interest.

Concurrently, tracking algorithms have gained increased prominence for investigating the evolution of mesoscale and synoptic scale features (e.g., Tracking Algorithm for Mesoscale Convective Systems (TAMS), Python FLEXible object TRacKeR (PyFLEXTRKR), etc.) (Núñez Ocasio and Moon 2024; Feng et al. 2023). For this work, the Tracking and Object-Based Analysis of Clouds Python package, or tobac, was used to track GLM-observed lightning in a Lagrangian framework, facilitating analysis of additional spatiotemporal attributes of lightning (Heikenfeld et al. 2019; Sokolowsky et al. 2024). This tool is particularly useful when investigating lightning in a pre-genesis environment, where tobac could track the evolution of clouds and lightning and their various spatiotemporal attributes, such as duration or distance from the best-track center. These attributes could then be linked to genesis-relevant processes, such as low-level vorticity generation or the development of a mid-level circulation.

This work uses the continuous, high-resolution data provided by GLM to characterize lightning through various spatiotemporal attributes in a pre-genesis environment. Previous studies that investigated lightning in pre-genesis disturbances in the North Atlantic were limited by their instruments and assessed lightning simply through flash rates. This work will expand the characterization of lightning beyond a flash quantity. Specifically, the area and optical energy attributes of lightning measured by GLM are hypothesized to inform relevant processes for genesis, such as small-area and low-energy lightning indicating the presence of strong updrafts in deep convection. Such a relationship has been established for Oklahoma supercells using LMAs, as in Bruning and MacGorman (2013), but has not been investigated for a pre-genesis environment using geostationary lightning observations. An object-based analysis enabled by the tobac algorithm further expands the suite of lightning attributes assessed in this environment, offering additional information, such

as lightning duration and distance to the center of a disturbance. Therefore, the wealth of data provided by GLM, in addition to the compositing and tracking methods provided by tobac, offers a novel and informative framework for characterizing lightning in a pre-genesis environment.

The thesis is organized as follows. The next section describes the datasets used in this analysis, including the cases considered, the methods for obtaining storm tracks and variables, as well as a discussion on data from GLM and ground-based radar. The next section also details the object-oriented approach enabled by tobac that was used to evaluate lightning characteristics in oceanic convection within a pre-genesis environment. Section 3 provides a physical interpretation of these lightning attributes through a radar analysis of Tropical Storm Claudette, in addition to evaluating broader trends in these attributes across three other cases of developing TCs. Section 4 concludes the thesis with a summary of findings and anticipated future applications of this expanded suite of lightning characteristics.

Chapter 2

Data and Methods

2.1 Cases

Four developing tropical disturbances in the North Atlantic basin were selected to evaluate the use of tobac and explore the relationship between lightning attributes and genesis. The four tropical disturbances eventually became Tropical Storm Claudette (2021), Hurricane Ida (2021), Hurricane Earl (2022), and Hurricane Beryl (2024). These cases were selected because they provided a range of environmental conditions that allowed for a broad initial investigation of lightning attributes prior to TC formation. NHC also noted the difficult genesis forecasts associated with all cases, except Beryl, in their respective Postseason Tropical Cyclone Reports (Papin and Berg 2022; Beven II et al. 2022; Blake 2023). Comparisons of the different aspects of these cases are shown in Table 2.1. The selected cases are shown to range in deep-layer shear magnitude, featuring low (Beryl), marginal (Ida and Earl), and high (Claudette) magnitudes. The cases also differed in terms of land interaction, as Earl and Beryl remained over open ocean, while Claudette and Ida skirted along the coasts of the Yucatan Peninsula and South America, respectively. Our results first examined lightning in pre-genesis Claudette to explore a physical interpretation of lightning characteristics. This physical interpretation was achieved by evaluating lightning features that varied in area and energy in relation to collocated radar data. Our analysis then targeted lightning within 200 km of the best-track center and 72 hours prior to genesis for pre-genesis Claudette and three other storms (i.e., Ida, Earl, and Beryl) to explore overall trends in these newly considered lightning attributes in a region inferred to be relevant for genesis.

2.2 Pre-Genesis Tracks

Official tracking of tropical disturbances by the NHC begins with the declaration of an area of investigation, or “invest”. This declaration sometimes occurs only a few days before genesis

Case	Genesis Date and Time	Max 850-250 hPa Wind Shear	Land Interaction
Claudette	June 19, 2021 0000 UTC	15 m s^{-1}	6/16 along the Bay of Campeche coast; 6/18 along the northern Gulf Coast
Ida	Aug. 26, 2021 1800 UTC	8 m s^{-1}	8/23-8/24 along the northern edge of South American coast
Earl	Sept. 2, 2022 1800 UTC	8 m s^{-1}	None
Beryl	June 29, 2024 0600 UTC	6 m s^{-1}	None

Table 2.1: Summary of tropical cyclone genesis characteristics across the four storm composite.

and may also be several days after the disturbance appears in satellite imagery. To extend the pre-genesis analysis period, the Automated Tropical Cyclone Forecasting System (ATCF) b-deck for invests and named storms was merged with an additional track source. This additional source advected the first position in the invest b-deck backward in time using the shallow Trajectory and Beta model (TABS; DeMaria et al. 2022). Merging these tracks into a single file then enabled the analysis of a tropical disturbance multiple days prior to genesis. Figure 2.1 shows the merged tracks for the four cases. This work focuses particularly on the period leading up to tropical storm genesis, as indicated by the tracks before the "X" marker. Additional storm-relative variables, such as deep-layer vertical wind shear, were obtained from ECMWF 5th Generation reanalysis (ERA5) fields for all times in the merged track (Hersbach et al., 2020). The merged track and its corresponding storm-relative variables were then linearly interpolated to five-minute intervals to match the time step used to process GLM data. The track and vertical wind shear vectors allowed for the examination of lightning in both a storm-centric and shear-relative reference frame.

Three days prior to genesis was used as the start of the analysis period, similar to Wang (2018). Genesis time and location were defined by the designation of a tropical storm (TS) by the NHC. Tropical storms are defined to have 1-minute maximum sustained winds of at least 17 m s^{-1} with sustained and organized deep convection surrounding a closed surface circulation. Most of the aforementioned studies that looked at lightning and convective intensity in tropical disturbances used tropical depression (TD) designation to define genesis; however, a TS designation was used in this study because a cyclone at this stage is typically better defined and easier to identify with

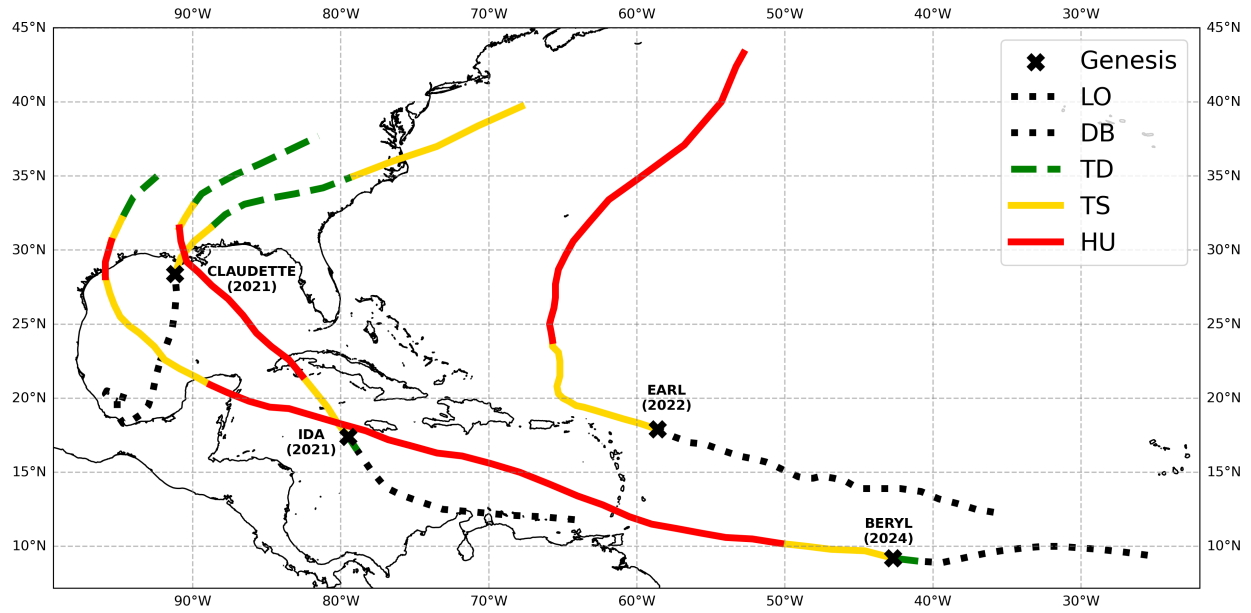

Figure 2.1: Tracks of the cases in the four storm composite. Tracks consisted of the Automated Tropical Cyclone Forecasting System (ATCF) b-deck for invests and named storms. The b-deck tracks were also merged with an additional track source that advected the first position in the invest b-deck backward in time using the shallow Trajectory and Beta model (TABS; DeMaria et al. 2022). This helped extend the pre-genesis analysis period. The location of TS genesis for each storm is shown as a black 'X'.

respect to observational uncertainty, as opposed to a TD whose main categorical difference to a TS lies in its maximum wind speed. The definition of genesis has minimal impact on the outcomes of this work, as two of the cases investigated never had tropical depression designations and were first identified as tropical storms (Claudette (2021) and Earl (2022)). Trends prior to the formation of a TD and TS for the other two cases (Ida (2021) and Beryl (2024)) will be discussed for the sake of comparison to prior work.

2.3 GLM

GLM is a near-infrared optical transient detector capable of mapping lightning in a temporally continuous manner. The spatial resolution of GLM ranges from ∼8 km at nadir to 14 km near the edge of the field of view (Goodman et al., 2013). GLM was designed to meet a 70% flash detection efficiency, and recent validation studies suggest this threshold has been met (e.g., Bateman and Mach 2020; Bateman et al. 2021). GLM data, which includes location, area, and energy,

is reported under a hierarchical classification structure of events, groups, and flashes. Goodman et al. (2013) defines these classifications as follows. Events represent a single pixel exceeding the background threshold during a single frame. Events serve as the base unit of data for GLM and are represented on an event grid shown in Figure 2.2a. The Lightning Cluster Filter Algorithm (LCFA) then clusters the event grid into groups and flashes based on spatial and temporal thresholds (Goodman et al., 2010). Lightning groups, which will be used for this work, are defined as one or more adjacent event pixels meeting the detection threshold in a single time frame (2 ms integration window). The LCFA outputs groups as centroid points, as shown in Figure 2.2b, which are associated with area and optical energy variables based on the underlying lightning event field. Flashes represent the highest level classification in the LCFA hierarchy and are defined as a set of groups that are no more than 330 ms and 16.5 km apart. Flash centroids are also associated with area and optical energy variables and reduce an array of events or a set of groups to a single point in both space and time.

The use of GLM group centroids for this project enabled the introduction of area as an attribute, which is otherwise unavailable for the base-level GLM event classification. Furthermore, GLM group centroids were able to better characterize the spatial extent of lightning that would otherwise be simplified into a single point with a GLM flash centroid, the top-level classification in the GLM hierarchy. The binned GLM group centroids in Figure 2.2c are shown to adequately represent the spatial extent of lightning when compared to the event grid (Figure 2.2a) and group centroids (Figure 2.2b). In contrast, using flashes to represent the same lightning at this time resulted in isolated flash centroids, which failed to capture the extent depicted by the event grid and group centroids. Maintaining the original spatial extent of the lightning was vital when considering the application of the tobac tracking algorithm to this data. Preserving the extent enabled accurate linking between tobac lightning features, thus providing the best possible characterization of the track and evolution of lightning measured by GLM.

GLM group centroids were binned onto a 0.05° by 0.05° uniform grid to facilitate tracking with tobac. Groups flagged by the LCFA were excluded from the binning, and no additional

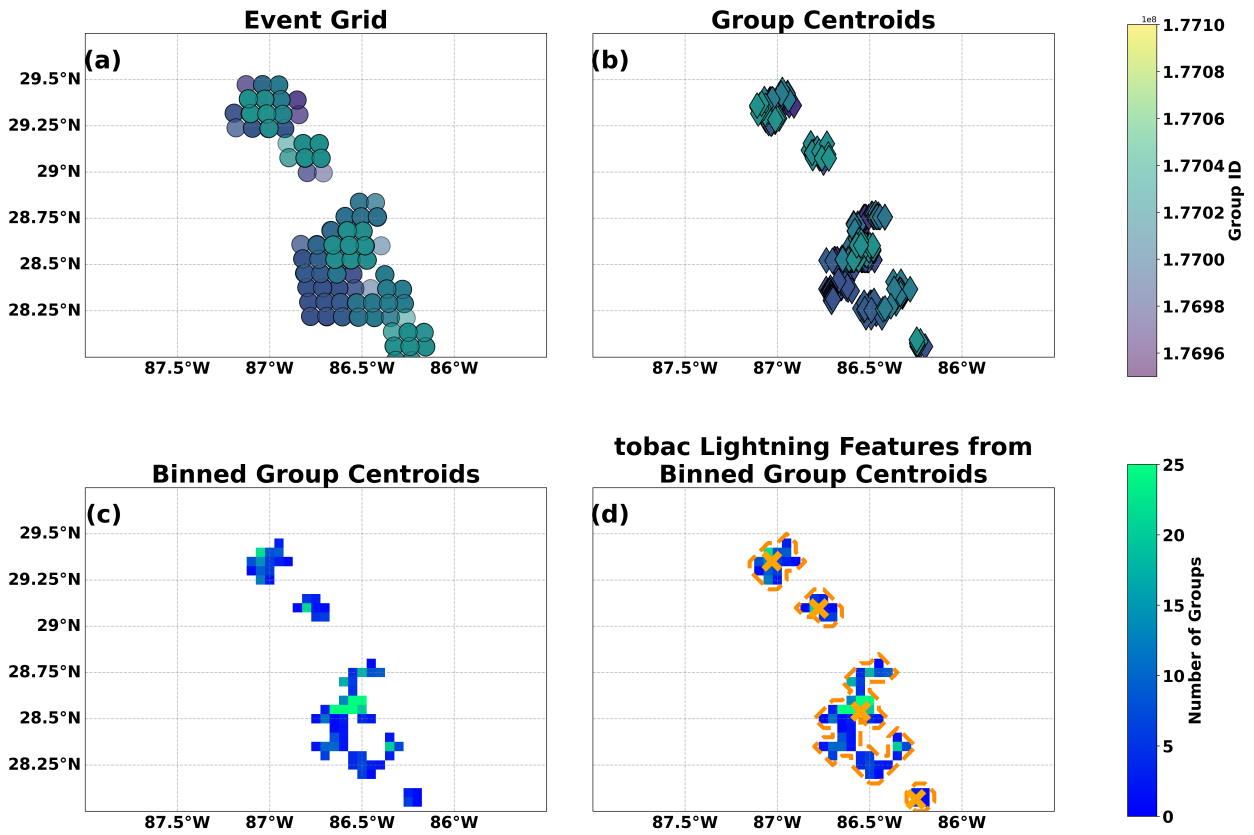

Figure 2.2: Five-minute accumulation of GLM data from pre-genesis Claudette (2021) on 18 June starting at 20:45 UTC. (a) Base-level GLM event grid colored by corresponding parent group ID. (b) GLM group centroids determined from the event grid in (a) and colored by group ID. (c) Binned GLM group centroids on a 0.05° by 0.05° uniform grid. (d) As in (c), with feature centroids and segmentation masks determined by tobac.

parallax correction was applied. Additional quality control was not warranted, as the LCFA has significantly improved since 2017, with 2% of lightning in Atlantic tropical cyclones flagged in 2021 (Trabing et al., 2024). The binned GLM group centroids were also binned temporally in five-minute intervals to streamline computational efficiency while still capturing the shorter, convective timescale of lightning.

Despite its significant advancements in lightning observations, GLM has various limitations compared to previous observing platforms, such as land-based mappers (e.g., Earth Networks Total Lightning Network). Compared to land-based mappers, GLM cannot measure polarity or flash type (e.g., cloud-to-ground, intracloud), and it has lower precision regarding lightning location (Marchand et al., 2019). All lightning sensors, including GLM, are known to have a strong diurnal

dependency. Specifically, GLM was designed for a daytime detection efficiency of ∼70% versus ∼90% overnight (Rudlosky et al., 2019). This design has the implication of making similar flashes appear larger and brighter at night compared to the day due to background solar illumination, although dynamic and thermodynamic influences may also play a role (Marchand et al. 2019; Rudlosky et al. 2019). Additionally, spaceborne lightning measurements can also be significantly impacted by the radiative impacts of clouds or the flash geometries themselves. For example, cloud-to-ground lightning may be associated with a lower total optical energy if the lightning occurred under what GLM sees as an optically thick cloud (Peterson et al., 2022). Nonetheless, the ability of GLM to offer continuous, high-resolution lightning data with high detection efficiency and relevant lightning attributes, such as optical energy, area, and location, marks a significant step forward in the field of lightning observations. Hence, GLM provides a valuable dataset for assessing lightning in a pre-genesis environment in the North Atlantic Basin.

2.4 Identifying and Tracking Lightning Features using tobac

The introduction of tobac enabled the consideration of additional spatiotemporal attributes of GLM-measured lightning in relation to genesis. By running the tobac tracking algorithm on the gridded group centroid field, tobac assigned feature centroids, contoured feature boundaries, calculated bulk statistics (i.e., feature mean group area), and ultimately linked these features together to determine cell lifetimes and create a lightning track data frame. An example of feature centroid and boundaries assigned by tobac for the binned group counts at a single step is shown in Figure 2.2d. This lightning track data frame enabled the ability to make additional, novel observations of the spatiotemporal aspects of lightning prior to genesis. An anticipated application of this framework was the identification of a long-lasting lightning cell indicative of strong updrafts and deep convection that occurred close to the disturbance's best-track low-level center. For the remainder of this paper, a lightning feature refers to a contiguous region of non-zero gridded GLM group counts that have been assigned a centroid and a segmentation mask at a single time step, as shown in Figure 2.2d. A lightning cell represents multiple lightning features linked over time.

Features and cells have the same attributes at each timestep; however, cells are also associated with a lifetime.

Tobac lightning features and cells were determined on the gridded group count data, with bulk statistics, such as mean group area and energy, calculated after the track data frame was created. Feature centroid locations were weighted by the binned group count within the feature. Watershed segmentation was then performed on these non-zero group count grid points to create a feature mask and calculate bulk statistics from the grid. Two additional measures were taken to ensure correct segmentation and, thus, accurate bulk statistics. The first measure accounted for weighted difference centroids that fell outside the feature boundaries, resulting in a failed segmentation for that feature. To resolve this issue, "ghost pixels" were introduced before segmentation if a centroid fell on a pixel without data. After segmentation, this pixel was removed to calculate bulk statistics. The second measure resolved the lack of diagonal segmentation capabilities in tobac v1.6. These capabilities were added via the introduction of a backend argument, as recommended by the tobac package managers (S. Freeman, 2025, personal communication).

Linking lightning feature centroids was found to be difficult at times, especially when features appeared to deviate from the mean flow due to the weighted centroid calculated from the group count. As a result, feature linking was performed with a maximum search radius of 15 km (allowing for a maximum lightning cell speed of 50 m s^{-1}). Rather than using the recommended 'predict' input for the method linking parameter, 'random' was used. The 'random' parameter input was found to perform better in linking features that were intuitively thought to belong to the same cell compared to using the 'predict' input. Therefore, using the 50 m s^{-1} maximum cell speed and 'random' parameters helped account for the unpredictable and "jumpy" nature of the lightning feature centroids driven by the weighted centroids. These parameters helped ensure long-duration cells were not broken into shorter tracks if the feature centroids were weighted farther away or deviated from the expected path between time steps. The subnetwork size was set to 100, providing a conditional limit on the number of features a cell could be linked to in the next time step. If this

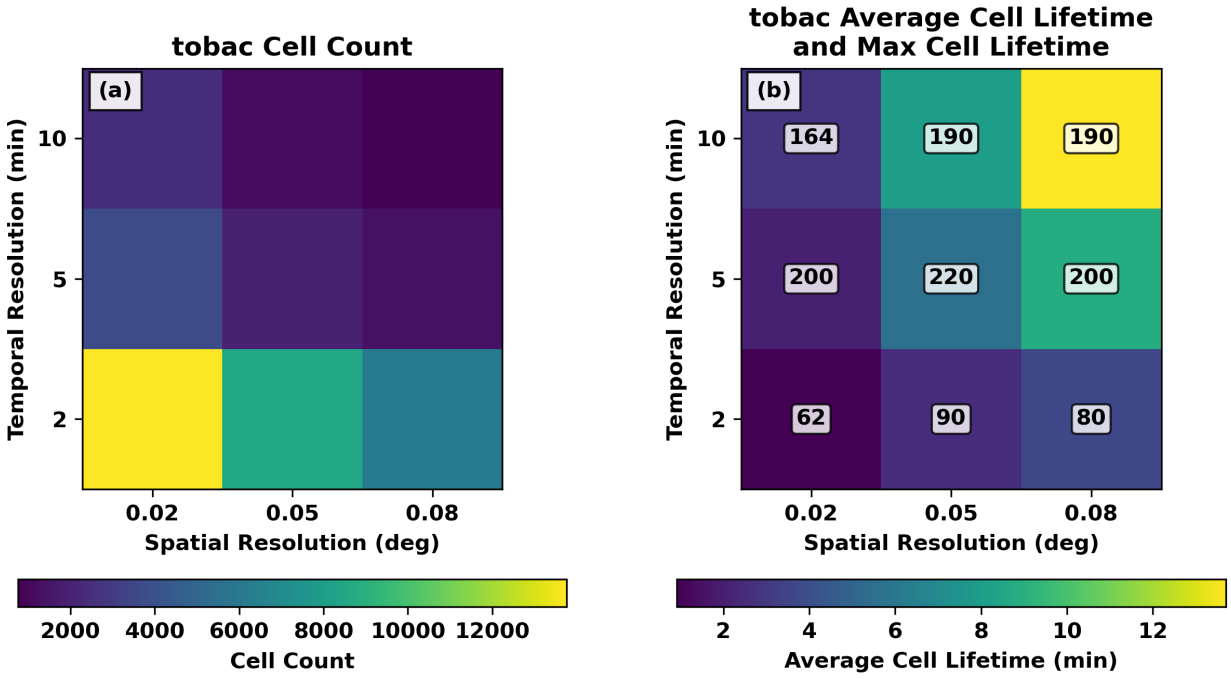

Figure 2.3: Dependence of tobac outputs on GLM group centroid bin resolution. Each resolution combination used lightning cells that were within 200 km of the center and 72 hours prior to genesis from the four storm composite. Bins of various resolution combinations shaded by (a) total cell count and (b) average cell lifetime with maximum cell lifetime overlaid on the bin (lifetimes in minutes).

limit was exceeded, the 15 km search radius was reduced by 5% until fewer than 100 features were identified or until the search radius was reduced below 3 km (20%).

The ability to quantify lightning duration through tobac tracking methods helped characterize lightning from a temporal perspective. One of the more important applications of this temporal variable was the ability to track long-duration cells with their evolving area and energy attributes. An idealized application of lightning lifetime was considered to be the identification of a long-duration lightning cell with attributes consistent with strong updrafts and deep convection. Such a cell would be hypothesized to serve as an efficient producer of low-level vorticity beneficial for genesis.

Classifications of lightning duration (i.e., short, medium, long) were based on the distribution of maximum cell lifetimes for cells in the four-storm composite that were within 200 km of the best-track center and 72 hours before genesis. Short-duration lightning cells (< five minutes) comprised 80% of the total distribution. In the context of our five-minute temporal binning, these cells

were only identified at a single time step. The 95th percentile of cell lifetimes corresponded to 25 minutes. As a result, medium-duration cells were defined as lasting between 5 and 20 minutes, while long-duration cells were 25 minutes or longer. Percentiles were used to define lifetimes as tobac tracking methods are sensitive to spatial and temporal resolution. Figure 2.3 illustrates cell counts and lifetimes for various resolution combinations using lightning cells within 200 km of the best-track center and 72 hours prior to genesis from the four storm composite. A finer spatial and temporal bin resolution resulted in a higher quantity of cells (Figure 2.3a) and shorter cell lifetimes (Figure 2.3b), a product of many distinct lightning features at each timestep. Coarser resolutions combined more GLM groups into individual lightning features at each timestep, reducing the total number of cells and allowing longer-lifetime cells to be resolved. Ultimately, a 0.05° by 0.05° uniform grid with a five-minute temporal resolution was selected, as it resolved long-duration cells while avoiding the under- or over-consolidation of GLM groups and variations in their attributes.

A land mask was also used to exclude lightning features that occurred over land. This mask helped account for lightning induced by land interaction, or in other words, lightning that would not have been indicative of the internal pre-genesis environment and processes in which this paper is interested. If, at any point, a lightning cell had a centroid $\leq$ 25 km from land, the entire cell was excluded from the track data frame. While not within the scope of this paper, land-induced convergence and convective initiation may be relevant for genesis, as shown by Park et al. (2017).

2.5 Ground-based Radar

As Figure 2.4 shows, Tropical Storm Claudette was a highly sheared TC whose genesis could be considered atypical as it interacted with an upper-level trough over Texas. However, its proximity to the northern Gulf Coast provided a case of genesis within range of the ground-based, dual-polarization Next Generation Weather Radar (NEXRAD) network in the GLM-observing era. Thus, Claudette offered a case in which electrified, oceanic convection in a pre-genesis environment could be analyzed using dual-polarization radar and GLM lightning data. More specifically,

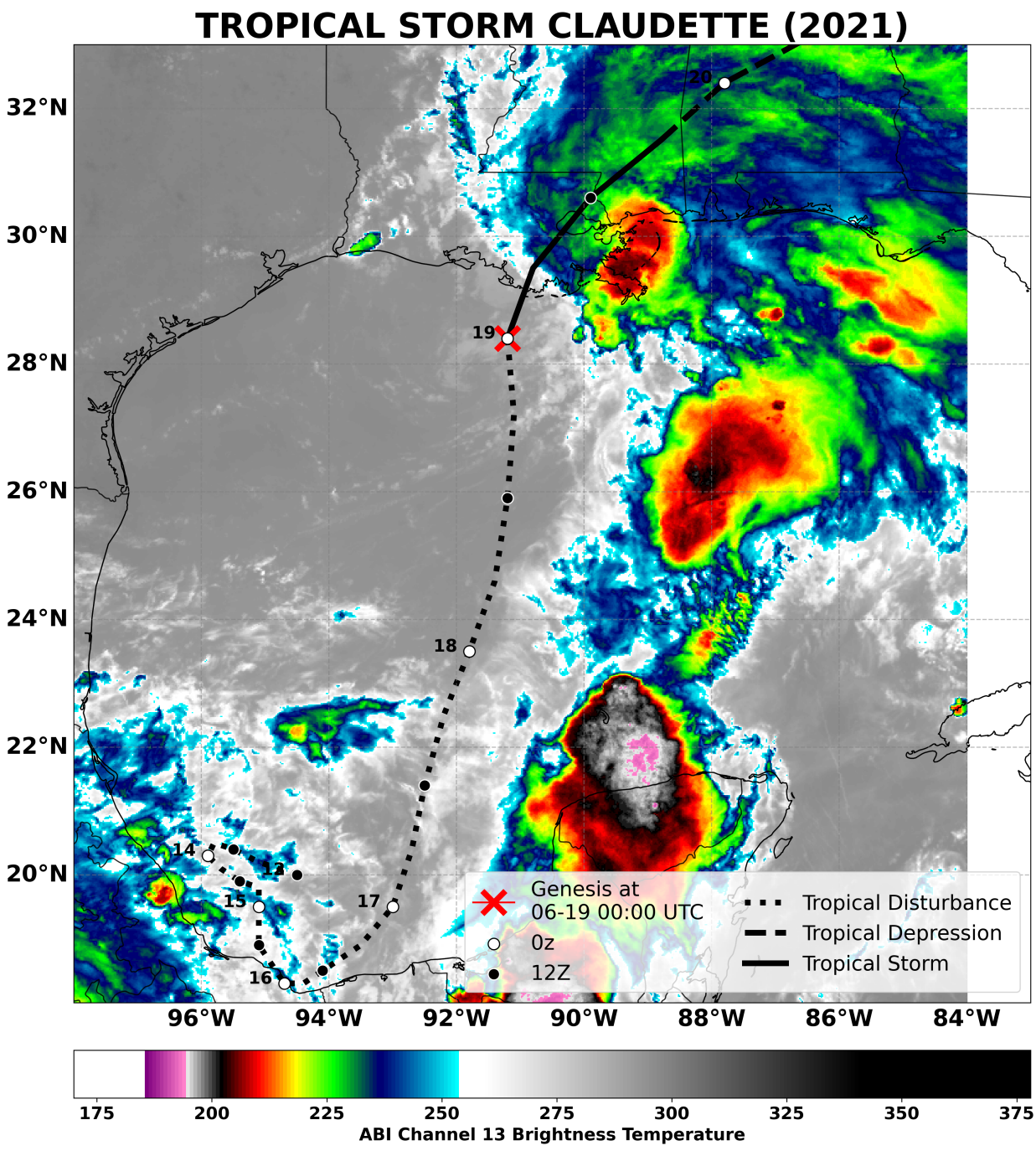

Figure 2.4: GOES-16 ABI Channel 13 image of Tropical Storm Claudette shown at the time of genesis on 19 June 2021 at 0000 UTC. Best-track and TABS-advected invest centers are also shown.

Claudette enabled the investigation of how variations in GLM-measured area and energy on a tobac feature basis related to convective strength and microphysical composition.

Figure 2.5 illustrates the composite radar reflectivity data provided by the KLIX, KMOB, and KEVX radars as an example of the broad radar coverage of Claudette's pre-genesis environment. Volumetric scans were downloaded from the Amazon Web Services NOAA-NEXRAD-Level 2 bucket for the three radars (NOAA National Weather Service (NWS) Radar Operations Center, 1991). These files were gridded and quality-controlled using the LROSE-Colette software, with specific differential phase (KDP) and particle identification (PID) fields also calculated using a KLIX sounding at 0000 UTC 19 June (DeHart et al., 2025). Gates with correlation coefficient values greater than 1 were omitted and differential reflectivity corrections were applied using the method detailed in Cunningham et al. (2013). Dual-polarization variables were plotted on a 1 km horizontal grid with 0.5 km vertical spacing. To obtain the composite radar profiles associated with variations in lightning area and energy, the binned GLM groups were regridded to match the 1 km gridded radar resolution and used to index the corresponding radar pixels. The sensitivity of the matched pixels was explored by adding a single-pixel buffer around the matched radar-GLM pixels. The results were not sensitive to this method, as the inclusion of buffered pixels yielded qualitatively similar results.

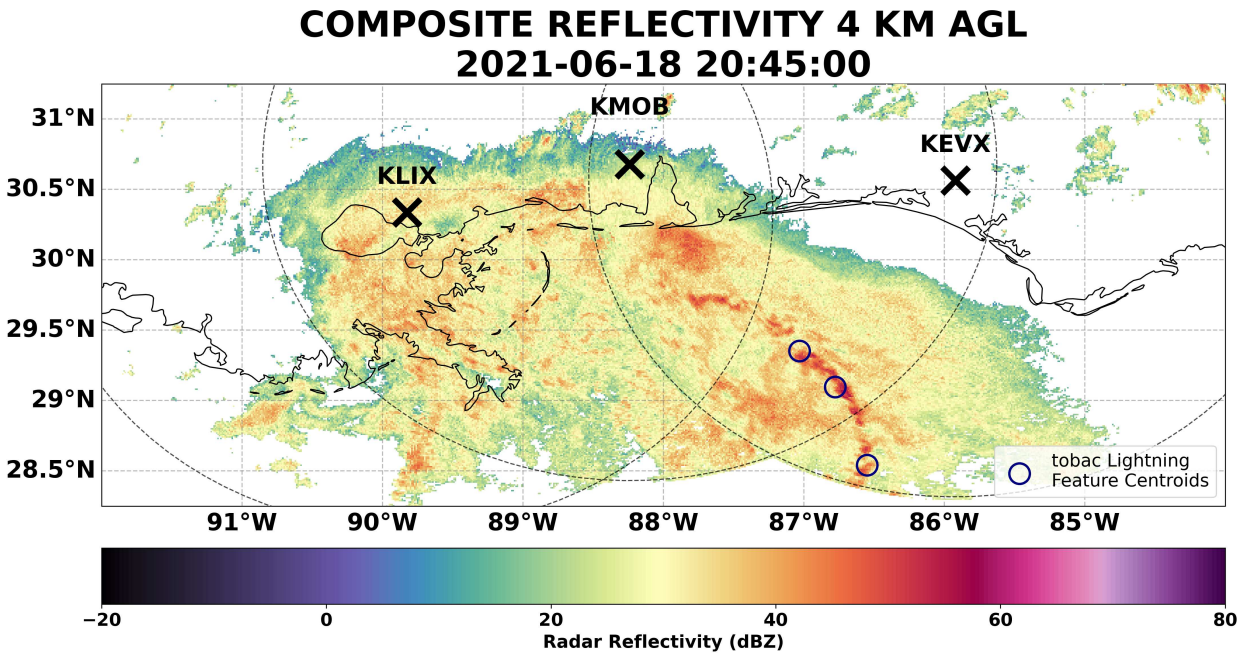

Figure 2.5: Tobac lightning feature centroids overlaid upon radar reflectivity at 4 km from KEVX, KLIX, and KMOB radars near 20:45 UTC on 18 June 2021. Reflectivity gridded at 1 km horizontal and 0.5 km vertical resolution by LROSE-Colette software. The dashed circles represent 250 km radii from each radar.

Chapter 3

Results

3.1 Claudette Case Study

3.1.1 Radar Characteristics of tobac Lightning Features

Tropical Storm Claudette offered a unique case study in which lightning attributes from GLM and the tobac framework could be assessed in a pre-genesis environment and compared with ground-based, dual-polarization radar data. Such an application enabled an evaluation of the microphysical composition and convective properties associated with our lightning attributes of interest. A total of 220 lightning features were identified to be within 250 km of the KLIX, KMOB, and KEVX radars in the 24 hours prior to Claudette's genesis. Due to the radar-based range thresholding, the majority of lightning features collocated with radar data in the pre-Claudette disturbance occurred away from the interpolated best-track invest center, with a mean distance of 440 km from the center for the 220 features. The majority of the 220 features also occurred eight hours prior to genesis. Limiting the features to within 250 km of the various radars allowed a maximum beam width of $\sim$4 km and ensured data was present between 4 and 9 km above ground level. Each feature was linked to the closest of the three radars. Selected radar scans were required to have a scan start time that fell within five minutes of the start of the five-minute lightning accumulation period (i.e., a lightning accumulation between 23:30 and 23:35 would be linked to a scan that started between 23:25 and 23:30). Because lightning-related processes originate in the mixed-phase region, radar scans needed to start before the accumulation to ensure the scans of the mid-levels were the closest possible to the associated lightning accumulation.

The relationship between the mean group area and the mean group energy for the 220 features in the radar subset is plotted in Figure 3.1, with a positive correlation evident between energy and area. As previously mentioned, Bruning and MacGorman (2013) tied lower-energy and smaller-area *flashes* measured by VHF LMAs to stronger convection in Oklahoma supercells, as opposed

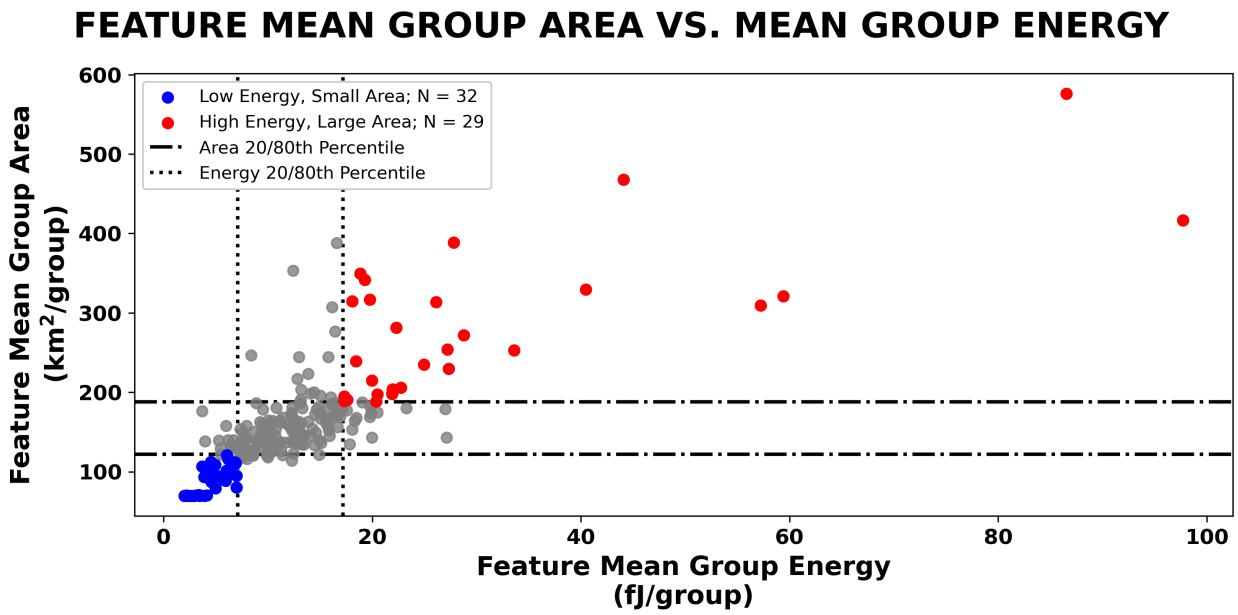

Figure 3.1: Relationship between mean group area and mean group energy in the 220-feature radar subset from pre-genesis Claudette. The vertical dotted lines represent the 20th and 80th percentile of mean group energy in the radar subset. The horizontal dash-dot lines represent the 20th and 80th percentile of the mean group area in the radar subset. Blue markers represent features that fell within the lowest 20th percentile for both mean group area and energy, while red markers represent features that fell within the highest 20th percentile for both mean group area and energy.

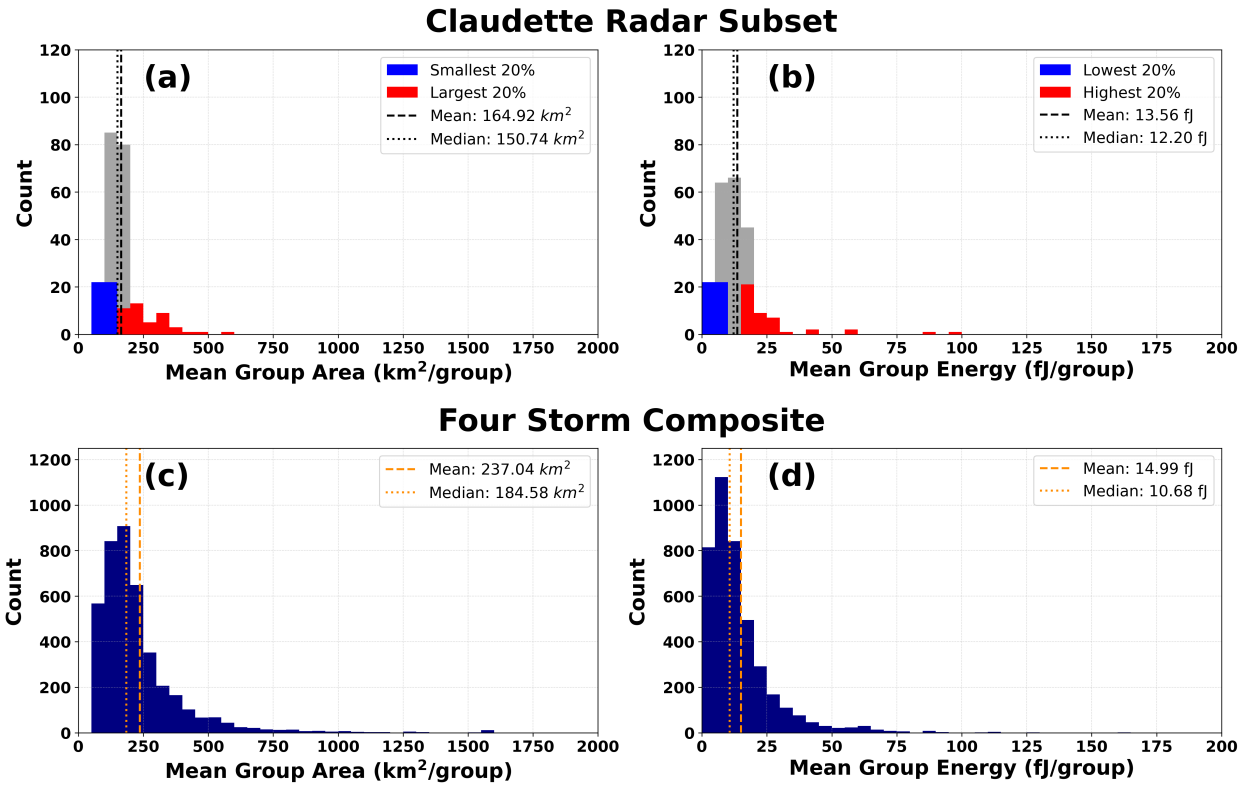

Figure 3.2: Histograms of (a) feature mean group area and (b) feature mean group energy for the subset of radar features in pre-genesis Claudette. (c) and (d) As in (a) and (b), but for lightning features within 200 km of the interpolated best-track invest center and 72 hours prior to genesis from the four cases in the composite.

to higher-energy and larger-area *flashes* being indicative of weaker convection and more stratiform processes. It is hypothesized that this relationship holds for GLM lightning *groups* in oceanic convection in a pre-genesis environment. Therefore, a distinction in convective strength should be able to be made when evaluating the vertical profiles of dual-polarization radar data associated with tobac lightning features that vary in area and energy. To evaluate this distinction in convective strength, lightning features were stratified by the top and bottom 20th percentile of mean group area and energy in the radar subset to define small-area, low-energy and large-area, high-energy features. This stratification resulted in 32 small-area, low-energy features and 29 large-area, high-energy features that were used in the composite radar analysis.

Figures 3.2a-b show the distribution of mean group area and energy from the 220-feature radar subset. The distributions of both variables are positively skewed and mainly dominated by smaller-

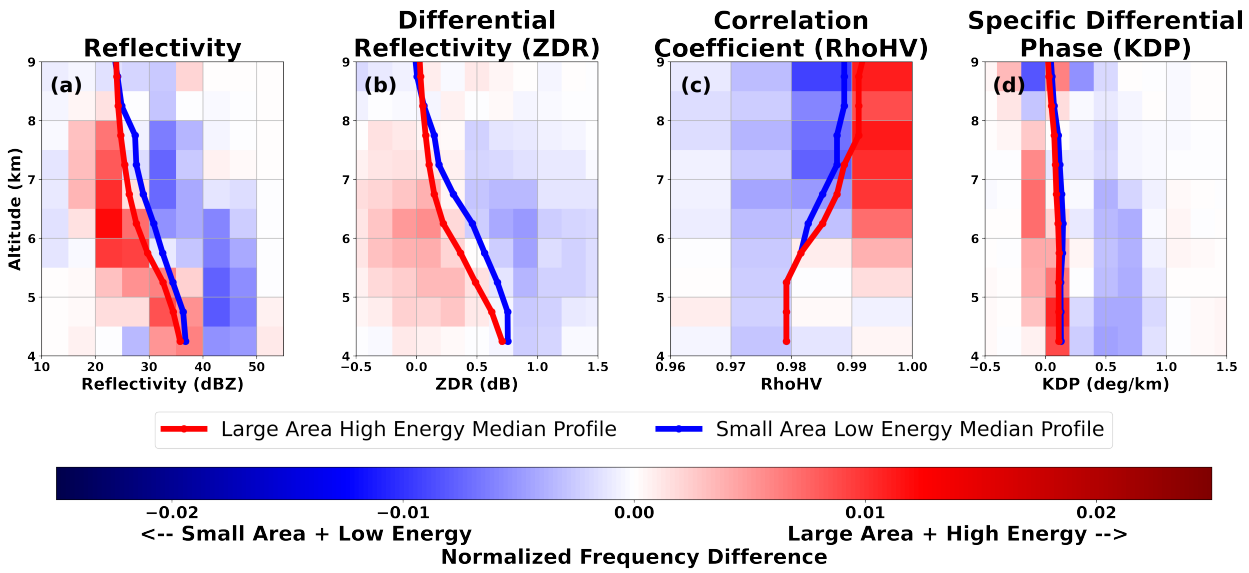

Figure 3.3: Composite vertical profiles of (a) reflectivity, (b) differential reflectivity, (c) correlation coefficient, (d) and specific differential phase from 4 to 9 km altitude. Features stratified by small-area, low-energy (blue), and large-area, high-energy (red) from the pre-genesis Claudette radar subset. Median profiles for each category are plotted in solid lines and overlaid upon altitude bins colored by normalized frequency difference.

area and lower-energy features. The two histograms shown in Figures 3.2c-d depict the distribution of the same variables, but for lightning features from the four-storm composite. The four-storm composite and its distribution of lightning features are discussed in further detail in the next section.

A composite of radar variables by altitude for the subset of features with collocated radar data in pre-genesis Claudette (from Figures 3.2a-b) is shown in Figure 3.3. The median values of the dual-polarization variables at each 0.5 km altitude bin are plotted using solid lines, overlaid on altitude bins shaded according to the normalized frequency difference. In general, Figures 3.3a-d show smaller-area, lower-energy features had higher reflectivities, more oblate particles, greater hydrometeor heterogeneity, and higher liquid water content above 4 km. Notably, features with smaller areas and lower energies had higher reflectivities (>30 dBZ) above the freezing level and throughout the mixed-phase region. According to the 0000 UTC KLIX sounding on 19 June, the freezing level was near 4.7 km and the -10C° level was near 6.8 km. Past work has consistently shown $\geq$30 dBZ values above -10C° to be associated with lightning, serving as an indicator of

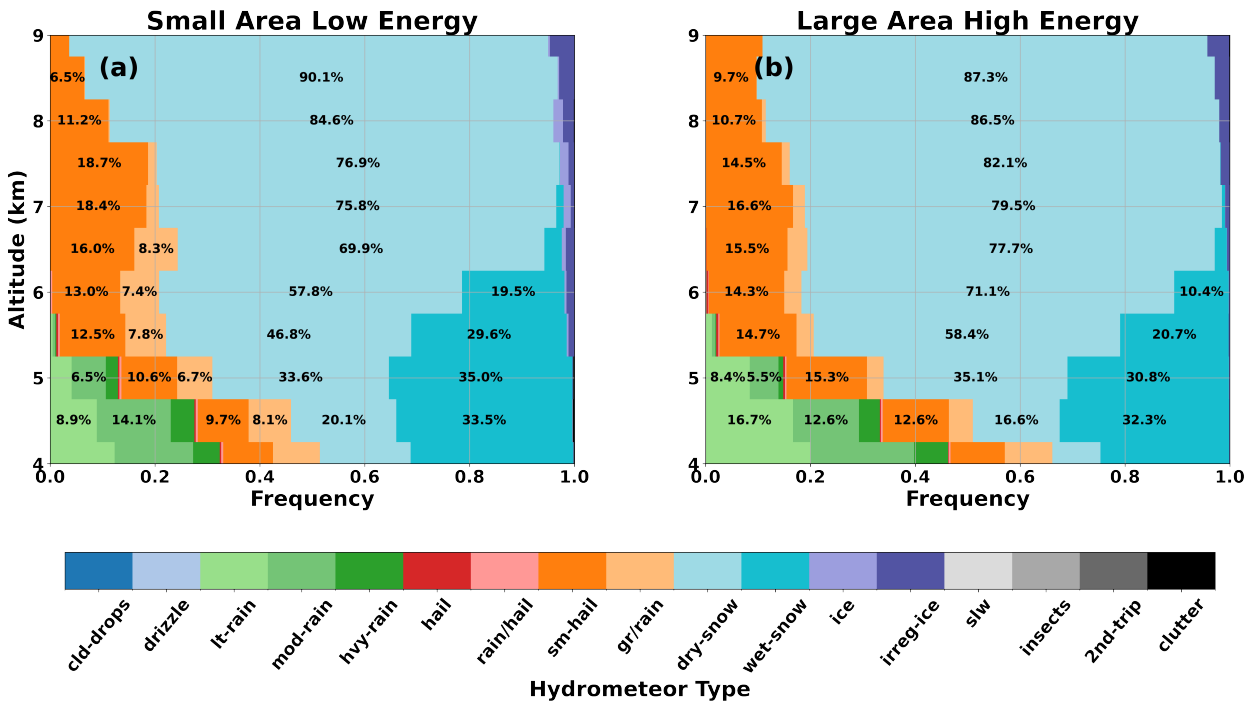

Figure 3.4: Composite vertical profiles of hydrometeor frequency at altitude bins from 4 to 9 km for (a) small-area, low-energy, and (b) large-area, high-energy features in the pre-genesis Claudette radar subset. Percentages are shown for hydrometeor frequencies greater than 5% at a given altitude bin.

sufficient hydrometeor concentration and updraft strength for charge generation (e.g., Petersen et al. 1996).

Greater physical intuition of the differences in the composite vertical distributions is possible when viewing all four variables in aggregate, typically best represented via PID. PID was performed via the LROSE RadxPID software, and a frequency of hydrometeor types for each altitude level can be found in Figure 3.4. Stronger convection and updrafts can be inferred with the greater frequency of graupel and rain between 4 and 7.5 km for small-area and low-energy lightning in comparison to large-area and high-energy lightning. Stronger updrafts in deep convection enable greater graupel production through riming by supercooled liquid droplets. The collision of graupel with smaller ice crystals in the presence of supercooled liquid water also facilitates charge separation between hydrometeors that is eventually discharged by lightning. Bruning and MacGorman (2013) provides a more detailed discussion of how these processes relate to frequent, small-area, and low-energy flashes.

Therefore, through the availability of ground-based, dual-polarization radar data in a pre-genesis environment, differences in convective strength and microphysical composition were shown for GLM-measured lightning that varied in area and energy. Specifically, smaller-area, lower-energy lightning features were indicative of stronger convection and an increased frequency of graupel. These variations, when evaluated through a novel, object-based framework, were found to match previous literature that established similar relationships in Oklahoma supercells (Bruning and MacGorman, 2013). In terms of the broader applications of these results, an informed assumption can be made about the underlying convective strength and microphysical composition of other oceanic lightning features in tropical disturbances based on their mean group area and energy values measured by GLM.

3.1.2 Pre-Genesis Lightning Trends

Findings from the radar case study offered a physical interpretation of lightning area and energy attributes measured by GLM. In applying the previous findings from the radar case study to regions within tropical disturbances presumed to be more relevant for genesis, a targeted analysis was conducted to evaluate the area, energy, and duration of lightning features within 200 km of the best-track invest center that occurred within 72 hours of genesis. Lightning features that met these criteria were accumulated from the four-storm composite shown in Table 2.1. For clarification, the vast majority of these 200 km features for Claudette were not found in the radar subset, which mainly consisted of features greater than 200 km from the best-track center. The distribution of the mean group area and energy of features in the four-storm composite is shown in Figures 3.2c-d. These distributions are shown to compare reasonably well with the Claudette radar subset distributions (Figures 3.2a-b), with a similar shape and positive skew. The four-storm composite showed a greater frequency of larger-area and higher-energy features, suggesting that the Claudette radar subset was characterized by a higher frequency of lightning associated with stronger convection. The median value of the four-storm composite for mean group area (184.58 km^2/group) and mean group energy (10.68 fJ/group) were selected as the threshold value for small versus large-area and

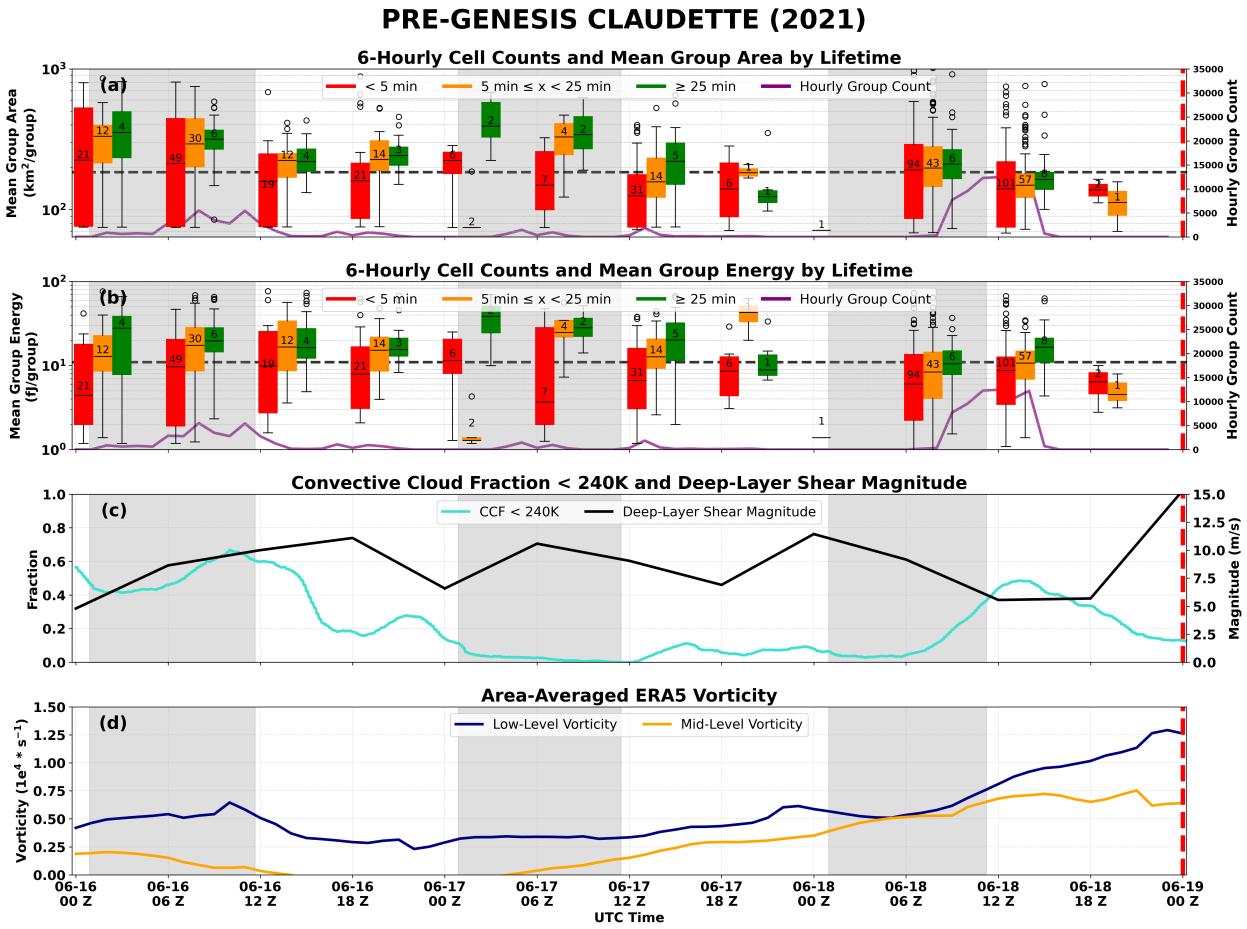

Figure 3.5: Lightning, convection, and dynamics-related variables within 200 km of the interpolated best-track invest center three days prior to Claudette's genesis. The dashed red line represents the time of TS genesis. Non-shaded and shaded regions represent local day and night, respectively. (a) Mean group area of lightning features binned by cell lifetime every six hours. Numbers in bins correspond to the count of lightning cells in respective six-hour periods for each lifetime classification. The dashed black line represents the median value of lightning features within 200 km in the four-storm composite. (b) As in (a), but for mean group energy. (c) Fraction of Channel 13 ABI brightness temperature pixels below 240 K and deep-layer shear magnitude. (d) Area-averaged vorticity within 200 km from ERA5 for 900-700 hPa (low-level) and 600-400 hPa (mid-level).

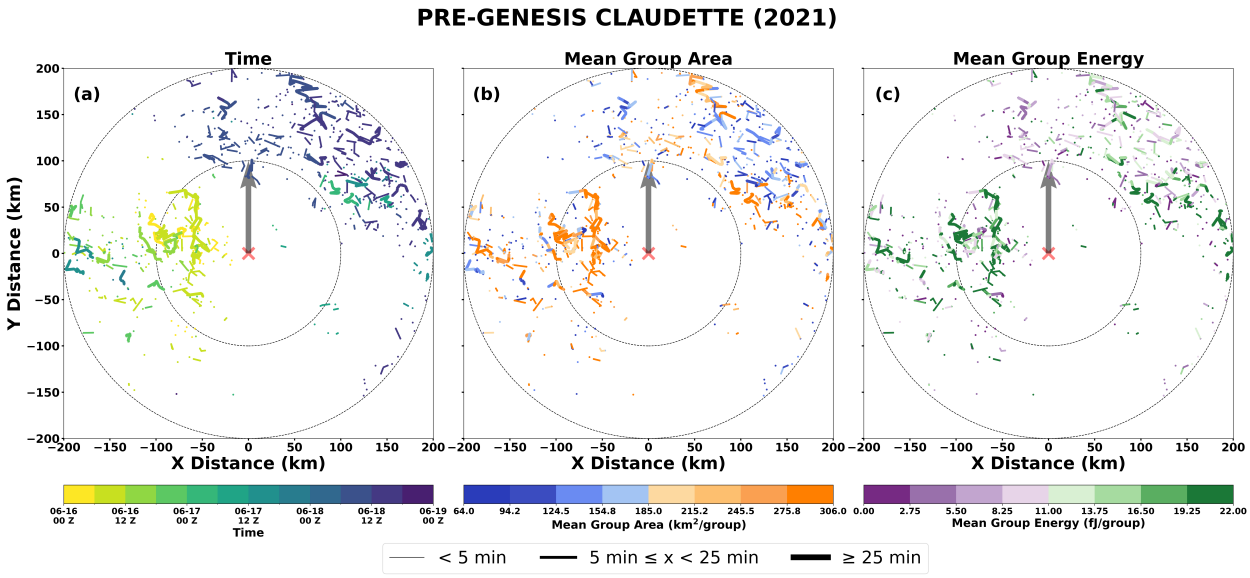

Figure 3.6: Pre-genesis Claudette lightning cell tracks within 200 km of the interpolated best-track invest center on a deep-layer shear-relative frame. Tracks are colored by (a) time until genesis, (b) mean group area, and (c) mean group energy.

low versus high-energy lightning. These median values corresponded well with the 20th percentile stratification in the radar subset and were consistent in magnitude with average GLM group observations over the open ocean in Rudlosky et al. (2019) (196 km^2 and 20 fJ).

Figure 3.5 illustrates lightning attributes and additional variables of interest over time within 200 km of the post-processed best-track invest center for Claudette. The attributes and variables include lightning mean group area and energy, GLM group count, deep-layer vertical wind shear, fraction of Advanced Baseline Imager (ABI) 10.3μm IR brightness temperature pixels below 240 K, and ERA5 low- and mid-level vorticity. Figures 3.5a and 3.5b show mean group area and energy values binned by lightning cell lifetimes every 6 hours. Lifetime bin assignments were determined by the maximum lifetime associated with a cell, with each feature throughout a cell's existence corresponding to a single point in the boxplot distribution. The black dashed line represents the median value of the mean group area or energy from the four-storm composite (including Claudette). This composite threshold is used for the remainder of the paper to characterize lightning as smaller (lower) or larger (higher) area (energy) for distributions in Figures 3.5a-b and tracks in Figures 3.6b-c. Hourly group counts are presented as an analogous quantity to the light-

ning flash count and rate observed in previous work, complementing the boxplots with a greater temporal resolution of lightning activity.

The convective cloud fraction in Figure 3.5c was defined as the percentage of ABI 10.3μm IR brightness temperature pixels below 240 K. Thiel et al. (2020) found that lightning measured by GLM often occurred when brightness temperatures were less than 240 K during two severe weather events over the continental US. This metric also provided a measure of convective cloud cover near the best-track center. Figure 3.5c also depicts deep-layer shear for the pre-Claudette disturbance, which ranged between 5 and 11 m s^{-1} in the pre-genesis period.

Low- and mid-level relative vorticity, shown in Figure 3.5d, were calculated by taking a 200 km radius area average from the 900-700 hPa and 600-400 hPa levels, respectively, around the interpolated best-track invest center. Lightning and convective cloud fraction in Figures 3.5a-c are intended to illustrate trends in convective coverage and intensity, with strong, deep convection known to be an effective producer of low-level vorticity, shown in Figure 3.5d. While ERA5-derived vorticity has considerable uncertainties, reanalysis products provided the only measure of vorticity available for the cases considered (Slocum et al., 2022).

Figure 3.6 provides spatial context to this feature-based analysis, showing lightning cell tracks within 200 km colored by (a) time, (b) mean group area, and (c) mean group energy. Tracks are plotted on a shear-relative, track-centered reference frame. Based on results from the radar case study in Claudette, lightning tracks in the darkest (i.e., blue and purple) colors across all three subplots (i.e., cells closer to time of genesis that are smaller in mean group area and lower in mean group energy) are hypothesized to be indicative of stronger convection and updrafts near the time of genesis. Colorbars in Figures 3.6b-c diverge from the composite median threshold to depict lightning that was smaller (lower) or larger (higher) in area (energy).

16 June featured substantial lightning activity overnight and throughout the day for the pre-Claudette disturbance as it drifted along the Mexican coast in the Bay of Campeche. Hourly group count in Figures 3.5a and 3.5b peaked and hovered near 5000 groups between 0600 and 1200 UTC. This 6-hour time period also featured a relative maximum in cell counts across all lifetime bins,

which was later exceeded on 18 June. During this peak in the group count, and overall throughout 16 June, medium- and long-duration cells were characterized by larger areas and higher energies, as indicated by their interquartile ranges primarily falling above the composite threshold value. This observation is also shown in Figure 3.6, which provides a better sense of the area and energy attributes for each lightning cell. Many of the thicker and longer lightning cell tracks during this time are orange and green in Figures 3.6b and 3.6c, indicative of larger-area and higher-energy lightning that was previously associated with weaker convection and stratiform processes in the radar analysis and prior studies. Lightning activity in the early morning of 16 June coincided with an absolute maximum in the convective cloud fraction for the analysis period ($\sim$60%), in addition to increasing deep-layer shear, as shown in Figure 3.5c. Despite the abundance of lightning and widespread coverage of colder cloud tops, Figure 3.5d shows minimal corresponding increases, and even decreases, in the low- and mid-level vorticity during this period. Decreases in mid-level vorticity, in particular, were unexpected, given the abundance of medium- and long-duration cells characterized by larger-area and higher-energy lightning. The disconnect between the presence of these lightning attributes and the decrease in mid-level vorticity during this period could be attributed to multiple factors, including the increasingly moderate to high levels of deep-layer shear, as well as the disturbance's proximity to land and potential dry air entrainment. The potential for lightning to be indicative of multiple mechanisms that both positively and negatively impact intensification and genesis is one of the reasons why Stevenson et al. (2018) investigated lightning in only favorable environments (i.e., low deep-layer wind shear, warm sea-surface temperatures, etc.).

Convective activity decreased from 16 to 17 June. The convective cloud fraction failed to surpass 20% while deep-layer shear remained between a moderate and high regime as the disturbance trekked across the Gulf. The pre-Claudette disturbance featured suppressed lightning activity on 17 June, with hourly group counts limited to relatively small bursts overnight and during the day. The medians of the short lifetime distributions were consistently below the composite threshold across almost all time bins on 17 June for both area and energy. In contrast, the medians and

distributions of the medium and long-duration bins appeared to vary throughout the day. Appreciably larger-area and higher-energy lightning was evident overnight, with that trend still present for longer-duration lightning in the 1200 UTC bin. While it is difficult to establish a definitive link, the presence of larger-area and higher-energy lightning in the medium and long-duration bins during observed increases in the mid-level vorticity is notable. The speculated link again relies on the knowledge that the mid-level circulation benefits from weaker convection and stratiform processes, which were suggested to be present based on the lightning attributes. The consistent presence of short-duration, small-area, low-energy lightning throughout 17 June, in addition to the long-duration cell characterized by similar attributes after 1800 UTC, is noted in the context of steadily increasing low-level vorticity during this period.

One of the more notable periods of lightning activity for the disturbance occurred overnight and into the morning on 18 June. As pointed out by Papin and Berg (2022), this overnight burst of convection "helped spawn a better-defined, though still broad, circulation farther to the north." In the two 6-hour windows between 0600 and 1800 UTC, the cell counts across all lifetime bins matched or exceeded the maxima observed earlier in the analysis period. The maxima in cell counts coincided with an absolute maximum in the hourly group count that consistently exceeded 10,000 groups per hour. The medians and interquartile ranges of all lifetime bins for area and energy were more tightly clustered near or below the composite threshold, indicating stronger convection and updrafts. The trends in these distributions translated to a greater frequency of darker colors (i.e., blues and purples) across the three track plots in the downshear right quadrant. To reiterate, these darker colors indicated the presence of small-area and low-energy lightning, suggesting stronger convection and updrafts with higher reflectivity and graupel concentrations aloft. Strong, deep convection has been well established as an efficient producer of low-level vorticity, which is found to increase substantially at this time, as shown in Figure 3.5d. Lightning between 1200 and 1800 UTC also occurred while the deep-layer shear held steady around 6 m s^{-1} - the lowest since 0000 UTC on 16 June. Concurrently, Figure 3.5c depicts a relative maximum ($\sim$45%) of the convective cloud fraction for this period.

3.2 Investigating Lightning Trends Across Multiple Storms

The Claudette case served two critical purposes for this work, as it first established relationships between lightning and underlying physical processes using collocated GLM and radar observations in a pre-genesis environment. These relationships were then used to interpret electrified convection that occurred prior to Claudette's genesis. However, it is difficult to generalize the results from Claudette to the pre-genesis stage of other disturbances for various reasons. These include the atypical genesis setup that led to Claudette's formation, which prominently featured high shear from an upper-level trough over Texas. Additionally, the electrified convective burst of interest occurred during the transition from night to morning on 18 June, during which the diurnally dependent GLM detection efficiency may have confounded findings regarding our variables of interest (Zhang and Cummins, 2020). Specifically, the greater background solar illumination during the day may have artificially shrunk group areas. Lightning energy did not appear to be higher overnight, as might have been expected, though. The second part of this work aims to apply the analysis techniques used with Claudette to a broader set of cases (Table 2.1) to assess the robustness of the methods in storms in different environments (i.e., lower deep-layer shear, different subbasins, and variations in convective organization).

Figures 3.7, 3.9, and 3.10 are similar to Figure 3.5, depicting the various variables of interest within 200 km for pre-genesis Ida (2021), Earl (2022), and Beryl (2024), respectively. The black dashed line represents the median value of mean group area or energy from the four-storm composite (including Claudette). Figure 3.8 shows lightning cell tracks for each storm colored by time, area, and energy, as in Figure 3.6.

3.2.1 Ida (2021)

Ida was selected as a case of interest due to its somewhat poor genesis forecast, as noted in Beven II et al. (2022), in addition to a notable burst of lightning activity in the 48 to 24 hours prior to genesis. Satellite fixes from the operational f-deck also suggested this period of lightning activity was associated with a shift in the disturbance's low-level center. The pre-Ida disturbance

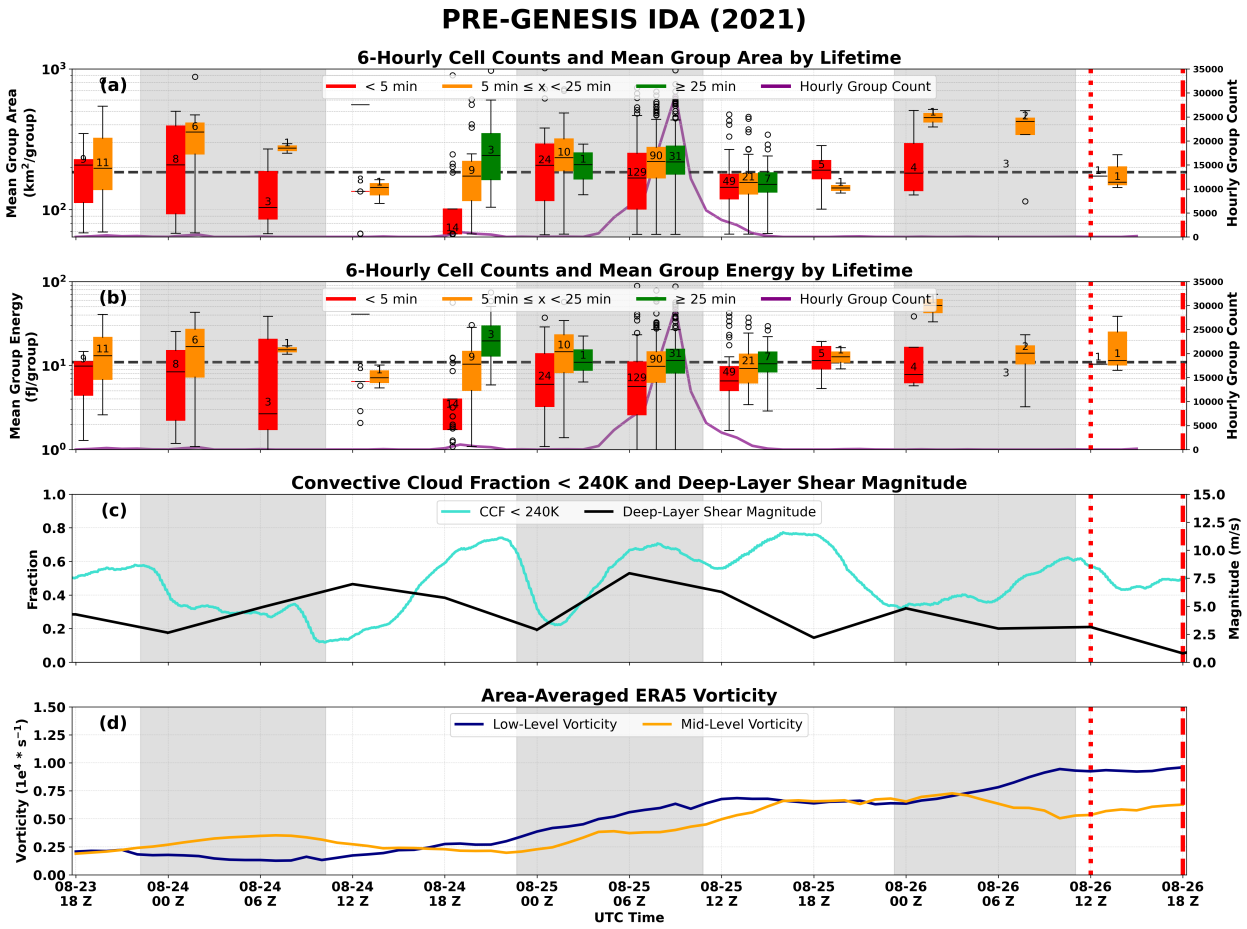

Figure 3.7: As in Figure 3.5, but for pre-genesis Ida. The red dotted line represents the time when a tropical depression formed.

experienced low to moderate deep-layer vertical wind shear during its pre-genesis period. The disturbance also interacted with land along the northern coast of South America from 23 August to early 25 August, where a broad area of low pressure was also present (Beven II et al., 2022).

Appreciable lightning activity first occurred in the pre-Ida disturbance after 1800 UTC on 24 August, with an enhanced period of lightning occurring between 0000 UTC and 1800 UTC on 25 August. During this time, Ida had the largest GLM group count out of the four cases, reaching over 30,000 groups around 0900 UTC (Figure 3.7a-b). A maximum in cell count for all three lifetime bins was also found at the 0600 UTC bin. In addition to the duration and quantity of lightning, their area and energy characteristics also illustrated trends of interest, as shown in Figures 3.7a-b. From 0000 to 1200 UTC on the 25th, the medians across most lifetime bins for mean group area were slightly above the composite median value, with some spread across the interquartile range. In contrast, between 1200 and 1800 UTC, the interquartile range across all bins shrank and sat below the composite median value, indicating that the majority of lightning at this time was characterized by smaller areas. Regarding the mean group energy, the medians across most lifetime bins were near or below the composite threshold between 0000 UTC and 1800 UTC, with tighter interquartile ranges below or straddling the composite threshold after 1200 UTC.

In connecting these attributes to a physical interpretation suggested by the radar analysis, lightning after 1200 UTC suggested the presence of stronger convection, characterized by lightning that was both smaller in area and lower in energy. Interpreting lightning from the boxplots is not as definitive for the overnight period between 0000 and 1200 UTC, but is aided by the track plots in Figures 3.8a-c. When examining individual tracks, long-duration cells indicative of both strong and weak convection are observed. These trends coincided with increases in low- and mid-level vorticity between 0000 and 1800 UTC.

At least two factors potentially influenced lightning observations during this period. The background illumination could have artificially decreased mean group areas and energy after 1200 UTC, although mean group energies appeared to remain consistent before and after sunrise. This lightning activity also coincided with the maximum deep-layer vertical wind shear (8 m s^{-1}) around

0600 UTC, which then decreased to 2 m s^{-1} by 1800 UTC. As previously mentioned, the abundance of lightning may have been a signal of detrimental environmental conditions (i.e., moderate deep-layer shear in this case) as much as it could have been a signal for beneficial processes at play for genesis. However, the increases in vorticity at the low- and mid-levels suggested the potential relevance of lightning in processes beneficial for Ida's genesis.

The pronounced period of lightning activity on 25 August was curiously followed by a lull in lightning activity directly preceding genesis. In contrast to the abundance of lightning cells across all lifetime bins immediately prior to Claudette's genesis, Ida featured very few short and medium-duration lightning cells (18 total) from 1800 UTC on 25 August to genesis at 1800 UTC on 26 August. Despite this limited lightning activity, there was a relative maximum in the convective cloud fraction of approximately 60% that occurred in the 6-12 hours before genesis, alongside an increase in low-level vorticity. While this may suggest Ida was a case that disproved the potential relevance of lightning and its attributes immediately preceding genesis, it is possible that the lightning activity and its attributes in the 24-48 hours prior to Ida's genesis were still important. As previously discussed, low- and mid-level vorticity increased with the abundance of lightning activity overnight on 24-25 August. Furthermore, previous work, such as Zawislak and Zipser (2014), has suggested that early convective and precipitation events can serve to beneficially modify a disturbance's environment in the days leading up to genesis.

3.2.2 Earl (2022)

Earl was selected for the composite as its genesis was well anticipated, but formation occurred much later than expected (Blake, 2023). Earl also offered a case of a broad and disorganized African easterly wave that faced low to moderate deep-layer vertical wind shear and did not interact with land.

Similar to Claudette, Figures 3.9a-b depict a disturbance with an abundance of lightning activity at the beginning of the analysis period. Blake (2023) noted that by 30 August, the pre-Earl disturbance was characterized by a broad area of elongated low pressure that faced moderate shear

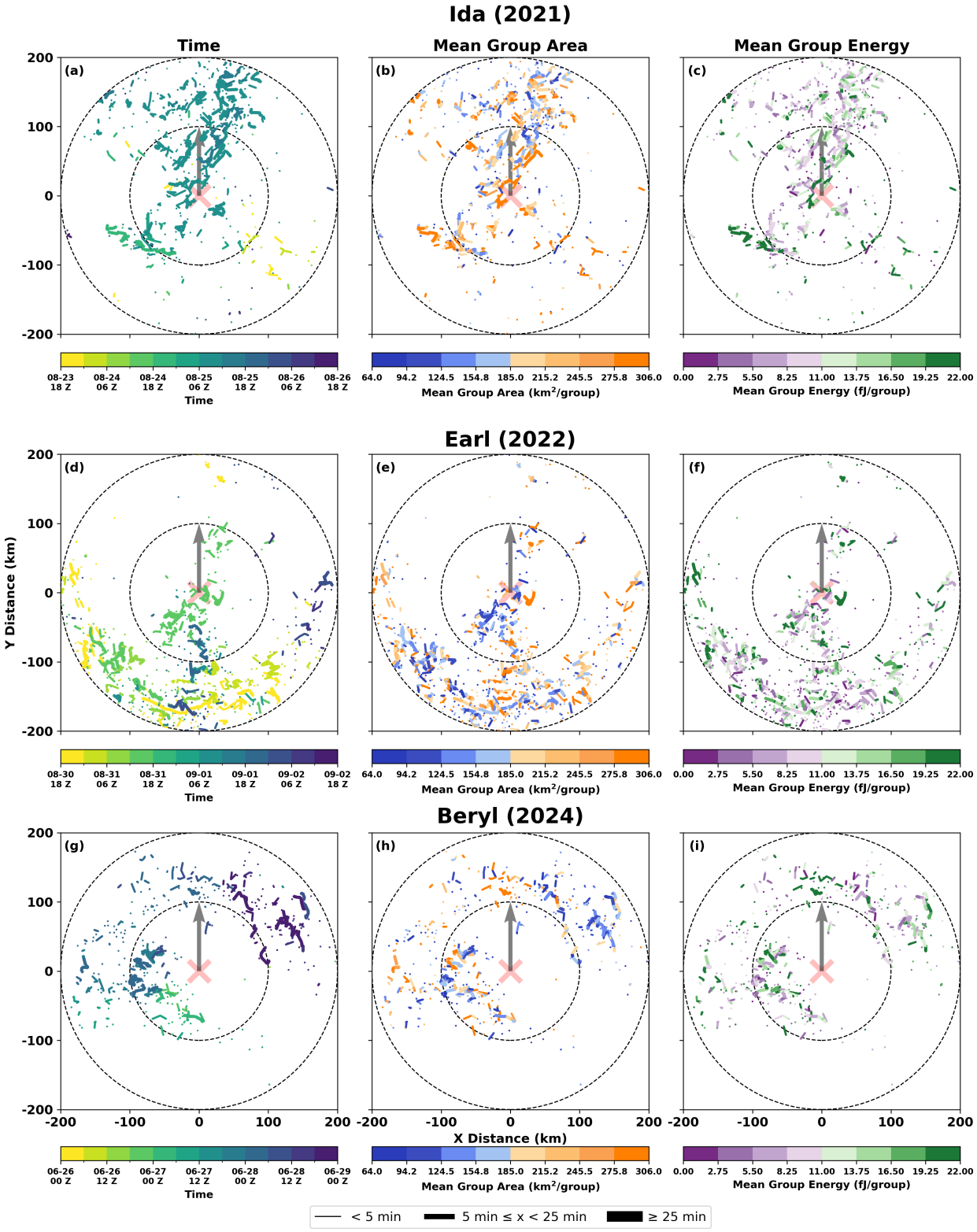

Figure 3.8: As in Figure 3.6, but for pre-genesis (a-c) Ida, (d-f) Earl, and (g-i) Beryl.

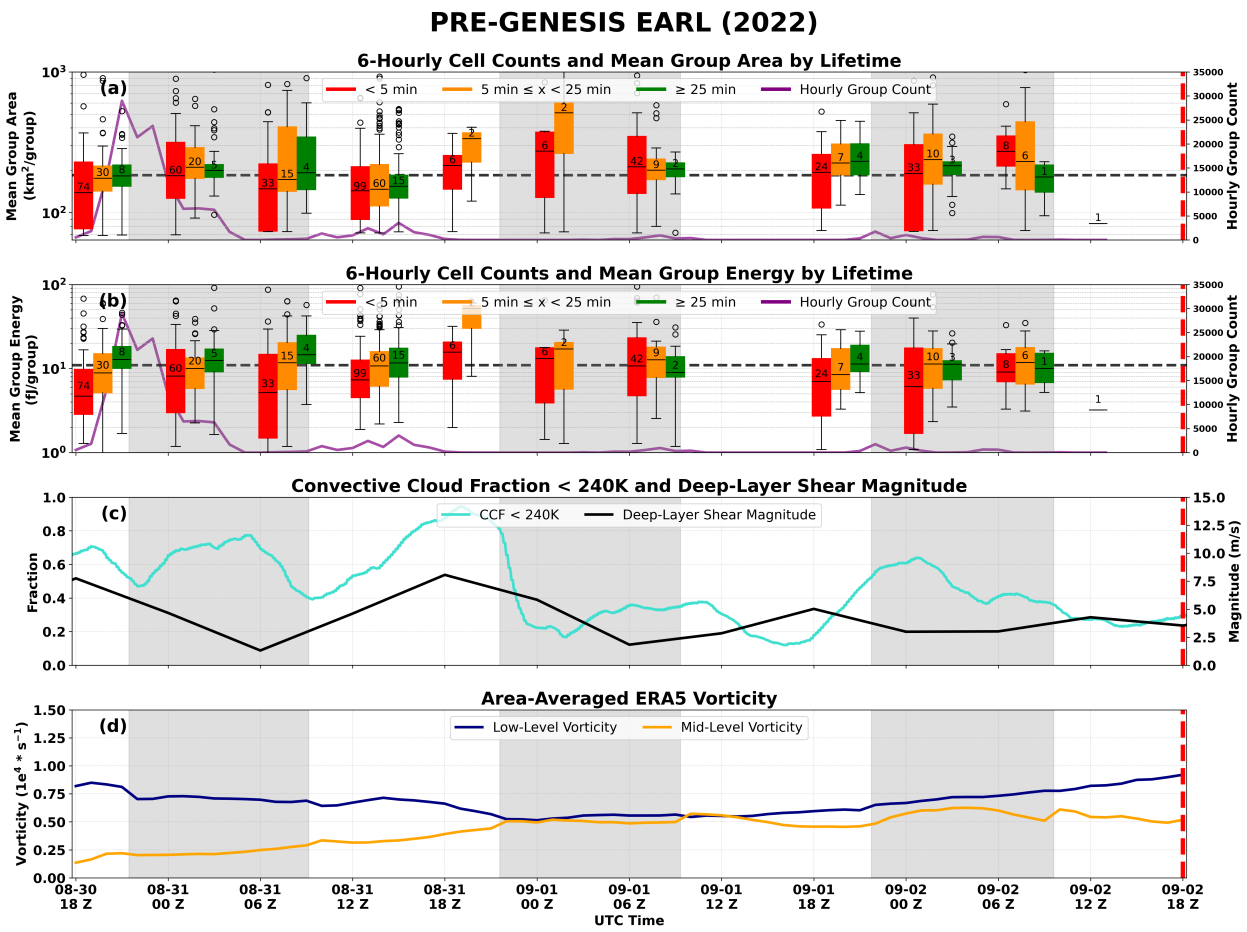

Figure 3.9: As in Figure 3.5, but for pre-genesis Earl.

($\sim$8 m s^{-1}) and a dry mid-level environment. These factors were noted to inhibit further convective organization of the disturbance until 1 September upon moving over warmer water. The abundance of lightning activity that coincided with these unfavorable conditions featured a prominent peak in the hourly GLM group count ($\sim$30,000 groups) around 2100 UTC on 30 August. The hourly group count later sharply decreased as the interpolated deep-layer shear magnitude fell below 2.5 m s^{-1} by 0600 UTC on 31 August. As the shear magnitude increased again shortly thereafter, small peaks in the hourly group count were also evident. Similar to Ida, Figures 3.9a-b do not communicate a definitive characterization of lightning between 1800 UTC on 30 August and 1200 UTC on 31 August. The most apparent trend during this time appeared to be short-duration bins mainly consisting of small-area and low-energy lightning. The track plots in Figures 3.8d-f better illustrate the lightning attributes during this early window and depict a mix of lightning indicative of stronger and weaker convection. Vorticity at the low- and mid-levels held steady during this period.

The boxplots provide a clearer characterization of the lightning after 1200 UTC on 31 August through 1 September. In particular, the period between 1200 and 1800 UTC on 31 August mainly consisted of smaller-area and lower-energy lightning as the shear magnitude increased to its maximum of the analysis period ($\sim$7.5 m s^{-1}). Cell counts across all lifetime bins also reached their maximum at this time. These takeaways are also clearly illustrated in Figures 3.8d-f, which show an abundance of small-area and low-energy tracks within 100 km of the best-track center.

The development of a mid-level circulation and overall increased organization on 1 September was not necessarily reflected in the vorticity time series in Figure 3.9d. However, these improvements in organization did coincide with some electrified convective activity in the early and late hours of 1 September. Lightning that occurred between 1800 UTC on 31 August and 0600 UTC on 1 September is shown in Figures 3.9a-b to have medians above the composite threshold for the few short and medium lifetime cells. These cells suggested that stratiform processes associated with large areas and high energy were more prominent during this period. In contrast, there was no clear trend in lightning attributes between 0600 and 1200 UTC on 1 September in both the boxplots and

composite tracks in Figures 3.8d-f. Area lifetime bin distributions and medians were centered near the composite threshold, similar to energy. No clear trends in the lightning attributes are found later on 1 September and into the day before genesis on 2 September. The shear-relative view of these cells in Figures 3.8d-f is also not able to provide a clearer characterization of the lightning during these times as it did for the earlier period of interest. Although the improved mid-level circulation was not captured in the vorticity time series, low-level vorticity increased on 2 September (Figure 3.9d). This increase occurred both during and after the period of overnight electrified convection that saw a 60% convective cloud fraction while facing reduced magnitudes of deep-layer shear.

Lightning attributes in the pre-Earl disturbance were thus somewhat similar to the Ida case. The initial large quantities of lightning at the beginning of the analysis period appeared to vary with the deep-layer wind shear, which ranged from moderate to low magnitudes. The attributes of the lightning during this period suggested a mix of both stronger and weaker convection, a finding that the track plots in Figures 3.8d-f illustrated particularly well in contrast to the boxplots in Figures 3.9a-b. The lightning observed between 30 and 31 August thus presented an additional case of lightning activity that appeared to be modulated by shear. Furthermore, lightning that occurred on 1-2 September coincided with improvements in the mid-level circulation and an overall enhancement in the convective organization. However, the lightning attributes observed during this time were not definitive enough to confidently call upon the relationships suggested in the radar analysis.

3.2.3 Beryl (2024)

Beryl was unlike the other cases considered for this composite, as it traversed a largely favorable environment, lending to a genesis that was well-forecast. The NHC Postseason Tropical Cyclone Report noted that the pre-Beryl disturbance first exhibited organized convection early on 27 June, becoming increasingly organized with a better-defined vorticity center early on 28 June (Beven II et al., 2025b). Notably, this improved organization coincided with an extended period of lightning activity from the late afternoon of 27 June into the early morning hours of 28 June.

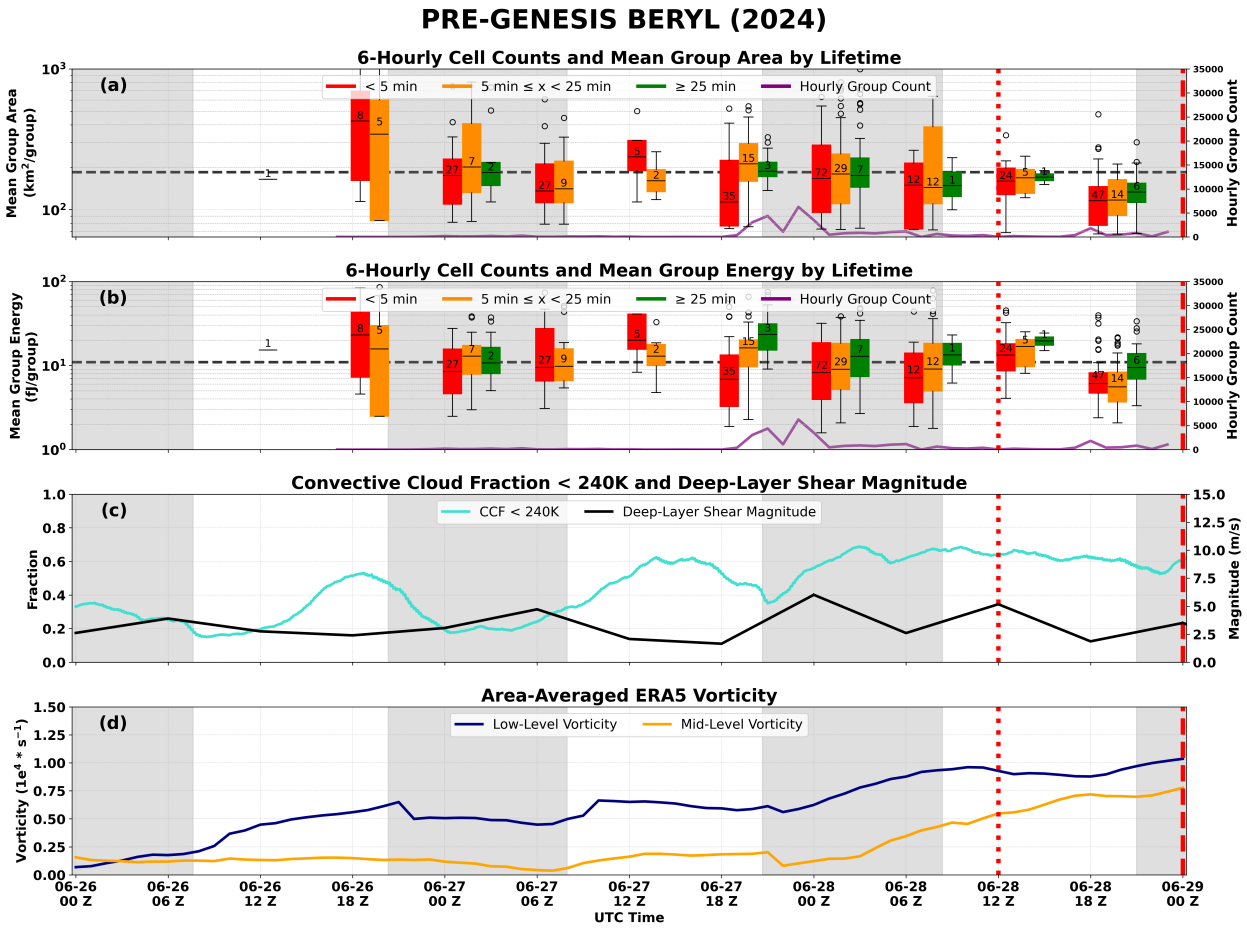

Figure 3.10: As in Figure 3.5, but for pre-genesis Beryl. The red dotted line represents the time when a tropical depression formed.

Lending further support to the potential significance of this lightning activity, a tropical depression was declared by 1200 UTC on 28 June. This overnight period was characterized by an absolute maximum in the hourly group count, shown in Figures 3.10a-b, in addition to maximum cell counts across all lifetime bins between 0000 and 0600 UTC. The medians of most lifetime bins held consistently near or below the composite threshold during this overnight period. This takeaway is evident in the track plots in Figures 3.8g-i, where lightning overnight on 27-28 June is shown primarily in the downshear left quadrant with many tracks characterized by smaller-area and lower-energy lightning. Particular interest is focused on the long-duration cell located 100 km to the left of the center, which was consistently characterized by smaller areas and lower energies throughout its lifetime, indicating a sustained period of strong updrafts and deep convection. Long-duration tracks, characterized by large areas and high energies, are also noted in this region. Despite the fact that lightning appears larger and brighter at night due to GLM's diurnal sensitivity, the distributions of area and energy remained consistently below or near the composite threshold overnight (3.10a-b). Lightning during this time also coincided with the maximum deep-layer shear magnitude ($\sim$6 m s^{-1}). From a genesis perspective, reanalysis vorticity in Figure 3.10d showed enhanced vorticity at the low- and mid-levels during this overnight lightning activity. The NHC Postseason Report also mentioned improved organization at this time (Beven II et al., 2025b).

Another period of interest occurred within six hours of genesis. Figures 3.10a-b show the second-highest cell counts for short and long-duration cells during this time. The medians for all lifetime bins of both variables are below the composite median threshold in addition to nearly their entire interquartile ranges. Relating the rather definitive nature of these attributes to the Claudette radar analysis, it appears lightning at this time was primarily indicative of strong updrafts and deep convection just prior to genesis. A key aspect of this lightning activity was that it occurred during a period of favorable deep-layer shear, implying that this lightning was an indicator of strong deep convection that was potentially beneficial for Beryl's genesis rather than being indicative of detrimental conditions, as suggested in other cases. It is still possible, however, that these area and energy values were influenced by the decreasing, but still present, sunlight at this time.

Lightning during this time is shown to be in the downshear right quadrant in Figures 3.8g-i. Of particular note are the two overlapping, long-duration tracks, which consistently showed smaller mean group areas. For group energy, one of the cells appeared to be characterized by a period of mean group energy slightly above the composite median. Most of the other cells that occurred in the six hours prior to genesis are also shown to have smaller mean group areas and lower mean group energies. Increases in the low-level vorticity coincided with this lightning, in line with our hypothesized link between the two.

Overall, the lightning during this six-hour period before genesis was considered an idealized example of the various lightning attributes we considered. Lightning at this time was characterized by small areas and low energies, suggesting the presence of strong updrafts and deep convection. Low-level vorticity, which can be generated through deep convection and is relevant for genesis, was also shown to increase, in line with our hypothesized link between lightning attributes and genesis-relevant developments. Lastly, the context of a favorable environment for this lightning served as an analogous application of the approach used in Stevenson et al. (2018), which controlled for detrimental factors, such as deep-layer shear, in mature TCs.

Chapter 4

Summary and Conclusions

The Geostationary Lightning Mapper aboard GOES-16 was used to investigate various spatiotemporal characteristics of lightning in a pre-genesis environment for the first time. In contrast to previous studies, which were limited by their observing platforms and characterized lightning in tropical disturbances through flash quantity, this work leveraged the continuous, high-resolution observations of additional attributes from GLM. Specifically, the area and optical energy of lightning groups measured by GLM were utilized to characterize convection in oceanic, pre-genesis environments. Furthermore, the tobac algorithm enabled the consideration of additional spatiotemporal attributes of lightning in this environment via compositing and tracking methods. These additional attributes included lightning duration and distance to the center of a disturbance. In applying an object-based analysis to lightning measured by GLM, a new framework was introduced that broadened the characterizations of lightning beyond a flash rate in a pre-genesis environment.

To assess how the expanded suite of lightning attributes related to physical processes in electrified, oceanic convection in a pre-genesis environment, this novel framework was first applied to Tropical Storm Claudette (2021). Claudette provided a case of tropical cyclogenesis within range of the ground-based, dual-polarization NEXRAD network along the northern Gulf Coast. Electrified convection was observed in a pre-genesis environment for multiple hours, enabling an evaluation of how variations in lightning area and energy were related to convective strength and microphysical composition in this unique environment. Tobac-identified lightning features with small mean group areas and low mean group energies were inferred to be indicative of stronger convection from composite vertical profiles of reflectivity, differential reflectivity, correlation coefficient, and specific differential phase. Small-area and low-energy tobac lightning features were also linked to higher frequencies of graupel and rain, as identified by the LROSE particle identification (PID) algorithm in the mixed-phase region. These findings were critical in that the area and energy attributes of oceanic lightning in a pre-genesis environment were suggestive of microphysi-

cal composition and convective strength. Furthermore, this connection, determined by applying the object-based framework to GLM observations, was in line with Bruning and MacGorman (2013), which found a similar relationship for lightning flashes in Oklahoma supercells measured by very high-frequency lightning mapping arrays. With these additional lightning attributes linked to convective strength and microphysical composition, a physical interpretation of lightning area and energy could then be applied to other pre-genesis cases and in regions presumed to have a greater impact on genesis.

Lightning that occurred within 200 km of the invest center and 72 hours prior to genesis was then investigated for the pre-Claudette disturbance. The physical processes suggested by lightning area and energy (e.g., small-area and low-energy lightning associated with stronger convection and enhanced low-level vorticity generation) were inferred to be more relevant for genesis in this region and time. Notably, the pre-Claudette disturbance was found to have an abundance of small-area, low-energy lightning in the 24 hours prior to genesis, suggesting the presence of stronger convection. This lightning activity of interest coincided with what Papin and Berg (2022) noted to be an overnight convective burst that helped spawn a better-defined low-level circulation, in addition to substantial increases in the ERA5 low-level vorticity. With that said, Claudette had multiple factors that advised caution in generalizing these trends. These factors included the moderate to high magnitudes of deep-layer shear that potentially had some influence in modulating lightning activity, in addition to the extratropical properties exhibited while developing into a TC in an atypical environment. These factors thus motivated an application of these expanded lightning attributes and their physical interpretations to a small composite of three other developing disturbances to assess broader patterns and evaluate their robustness.

The spatiotemporal characteristics of lightning were investigated in the disturbances that became Ida (2021), Earl (2022), and Beryl (2024). These disturbances exhibited differences in deep-layer vertical wind shear, timing of lightning activity relative to the diurnal cycle, and other factors such as land interaction, genesis location, and convective organization. The presence of small-area and low-energy lightning associated with stronger updrafts and deep convection was noted

for all three cases, specifically within 72 hours of genesis and within 200 km of the best-track center. Large-area and high-energy lightning, which was found to be consistent with weaker convection and stratiform processes, was also present. Additionally, there were multiple instances of lightning attributes coincident with genesis-relevant processes that were hypothesized to be related (i.e., the generation of low-level vorticity via deep convection, as identified by small-area and low-energy lightning). The six hours preceding Beryl's genesis provided an example of these coinciding occurrences, as small-area and low-energy lightning were present during increases in reanalysis low-level vorticity. The context of an otherwise favorable dynamic and thermodynamic environment helped to isolate this lightning from other potentially detrimental factors.

More work is needed to evaluate these lightning attributes in a larger composite of pre-genesis disturbances. Questions remain regarding the role of environmental factors, such as vertical wind shear and aerosol concentration, on the frequency and characteristics of lightning in tropical disturbances. Controlling for different factors, as Stevenson et al. (2018) did when investigating lightning in mature TCs under favorable conditions, would be particularly of interest. Better quantification of the impact of background solar illumination would also enable more accurate characterizations of trends in lightning area and energy that would eliminate artifacts introduced by the sensor's diurnal-based detection. Ongoing work is being conducted to evaluate whether the additional lightning variables presented here can be used as discriminators for distinguishing between developing and non-developing disturbances.

Bibliography

Bateman, M., and D. Mach, 2020: Preliminary detection efficiency and false alarm rate assessment of the Geostationary Lightning Mapper on the GOES-16 satellite. *Journal of Applied Remote Sensing*, **14 (3)**, 032 406, https://doi.org/10.1117/1.JRS.14.032406.

Bateman, M., D. Mach, and M. Stock, 2021: Further investigation into detection efficiency and false alarm rate for the geostationary lightning mappers aboard GOES-16 and GOES-17. *Earth and Space Science*, **8 (2)**, e2020EA001 237, https://doi.org/https://doi.org/10.1029/2020EA001237.

Bell, M. M., and M. T. Montgomery, 2019: Mesoscale processes during the genesis of Hurricane Karl (2010). *J. Atmos. Sci.*, **76 (8)**, 2235–2255, https://doi.org/10.1175/JAS-D-18-0161.1.

Beven II, J. L., L. Alaka, and C. Fritz, 2025a: National Hurricane Center tropical cyclone report: Hurricane Milton (5–10 October 2024). NHC Tech. Rep. AL142024, 72 pp. URL https://www.nhc.noaa.gov/data/tcr/AL142024_Milton.pdf.

Beven II, J. L., C. Fritz, and L. Alaka, 2025b: National Hurricane Center tropical cyclone report: Hurricane Beryl (28 June–9 July 2024). NHC Tech. Rep. AL022024, 76 pp. URL https://www.nhc.noaa.gov/data/tcr/AL022024_Beryl.pdf.

Beven II, J. L., A. Hagen, and R. Berg, 2022: National Hurricane Center tropical cyclone report: Hurricane Ida (26 August–1 September 2021). NHC Tech. Rep. AL092021, 163 pp. URL https://www.nhc.noaa.gov/data/tcr/AL092021_Ida.pdf.

Blake, E. S., 2023: National Hurricane Center tropical cyclone report: Hurricane Earl (2–10 September 2022). NHC Tech. Rep. AL062022, 18 pp. URL https://www.nhc.noaa.gov/data/tcr/AL062022_Earl.pdf.

Bruning, E. C., and D. R. MacGorman, 2013: Theory and observations of controls on lightning flash size spectra. *J. Atmos. Sci.*, **70 (12)**, 4012–4029.

Cunningham, J. G., W. D. Zittel, R. R. Lee, R. L. Ice, and N. P. Hoban, 2013: Methods for identifying systematic differential reflectivity (Zdr) biases on the operational WSR-88d network. *36th Conference on Radar Meteorology*, Amer. Meteor. Soc., Breckenridge, CO, 9B.5. [Available online at https://ams.confex.com/ams/36Radar/webprogram/Paper228792.html].

DeHart, J., M. Dixon, B. Javornik, M. Bell, T.-Y. Cha, A. DesRosiers, and W.-C. Lee, 2025: nsf-lrose/lrose-releases: lrose-colette-20250105. Zenodo, URL https://doi.org/10.5281/zenodo.14624762, https://doi.org/10.5281/zenodo.14624762.

DeMaria, M., and Coauthors, 2022: The national hurricane center tropical cyclone model guidance suite. *Wea. Forecasting*, **37 (11)**, 2141–2159.

Feng, Z., J. Hardin, H. C. Barnes, J. Li, L. R. Leung, A. Varble, and Z. Zhang, 2023: PyFLEX-TRKR: A flexible feature tracking python software for convective cloud analysis. *Geoscientific Model Development*, **16 (10)**, 2753–2776.

Gall, R., J. Franklin, F. Marks, E. N. Rappaport, and F. Toepfer, 2013: The Hurricane Forecast Improvement Project. *Bull. Amer. Meteor. Soc.*, **94 (3)**, 329–343, https://doi.org/10.1175/BAMS-D-12-00071.1.

Goodman, S. J., D. Mach, W. J. Koshak, and R. J. Blakeslee, 2010: GLM Lightning Cluster-Filter Algorithm (LCFA). Algorithm theoretical basis document, NOAA. URL https://www.star.nesdis.noaa.gov/goesr/documents/ATBDs/Baseline/ATBD_GOES-R_GLM_v3.0_Jul2012.pdf, 73 pp.

Goodman, S. J., and Coauthors, 2013: The GOES-R Geostationary Lightning Mapper (GLM). *Atmos. Res.*, **125**, 34–49.

Heikenfeld, M., P. J. Marinescu, M. Christensen, D. Watson-Parris, F. Senf, S. C. van den Heever, and P. Stier, 2019: tobac 1.2: towards a flexible framework for tracking and analysis of clouds in diverse datasets. *Geoscientific Model Development*, **12 (11)**, 4551–4570.

Hendricks, E. A., M. T. Montgomery, and C. A. Davis, 2004: The role of "vortical" hot towers in the formation of Tropical Cyclone Diana (1984). *J. Atmos. Sci.*, **61 (11)**, 1209–1232.

Hersbach, H., and Coauthors, 2020: The ERA5 global reanalysis. *Quart. J. Roy. Meteor. Soc.*, **146 (730)**, 1999–2049.

Houze, R. A., W.-C. Lee, and M. M. Bell, 2009: Convective contribution to the genesis of Hurricane Ophelia (2005). *Mon. Wea. Rev.*, **137 (9)**, 2778–2800, https://doi.org/10.1175/2009MWR2727.1.

Leary, L. A., and E. A. Ritchie, 2009: Lightning flash rates as an indicator of tropical cyclone genesis in the eastern North Pacific. *Mon. Wea. Rev.*, **137 (10)**, 3456–3470.

Leppert, K. D., D. J. Cecil, and W. A. Petersen, 2013a: Relation between tropical easterly waves, convection, and tropical cyclogenesis: A Lagrangian perspective. *Mon. Wea. Rev.*, **141 (8)**, 2649–2668.

Leppert, K. D., W. A. Petersen, and D. J. Cecil, 2013b: Electrically active convection in tropical easterly waves and implications for tropical cyclogenesis in the Atlantic and east Pacific. *Mon. Wea. Rev.*, **141 (2)**, 542–556.

Mac Home, F., 2022: Research note | November 9, 2022 Migration to environmentally risky areas: A consequence of the pandemic share.

Marchand, M., K. Hilburn, and S. D. Miller, 2019: Geostationary Lightning Mapper and Earth Networks lightning detection over the contiguous United States and dependence on flash characteristics. *Journal of Geophysical Research: Atmospheres*, **124 (21)**, 11 552–11 567.

Marks, F., N. Kurkowski, M. DeMaria, and M. Brennan, 2019: Hurricane Forecast Improvement Program five-year plan: 2019–2024: Proposed framework for addressing section 104 of the Weather Research Forecasting Innovation Act of 2017. NOAA, 86 pp. Https://hfip.org/sites/default/files/documents/hfip-strategic-plan-20190625-final.pdf.

Montgomery, M. T., M. Nicholls, T. Cram, and A. Saunders, 2006: A vortical hot tower route to tropical cyclogenesis. *J. Atmos. Sci.*, **63 (1)**, 355–386.

NOAA National Centers for Environmental Information, 2025: U.S. billion-dollar weather and climate disasters. Accessed: 2025-04-25, https://www.ncei.noaa.gov/access/billions/, https://doi.org/10.25921/stkw-7w73.

NOAA National Weather Service (NWS) Radar Operations Center, 1991: NOAA Next Generation Radar (NEXRAD) level 2 base data. Accessed: 2025-04-25, NOAA National Centers for Environmental Information, https://doi.org/10.7289/V5W9574V.

Nolan, D. S., 2007: What is the trigger for tropical cyclogenesis. *Aust. Meteor. Mag.*, **56 (4)**, 241–266.

Núñez Ocasio, K. M., and Z. L. Moon, 2024: TAMS: A tracking, classifying, and variable-assigning algorithm for mesoscale convective systems in simulated and satellite-derived datasets. *Geoscientific Model Development*, **17 (15)**, 6035–6049.

Papin, P. P., and R. Berg, 2022: National Hurricane Center tropical cyclone report: Tropical Storm Claudette (19–22 June 2021). NHC Tech. Rep. AL032021, 41 pp. URL https://www.nhc.noaa.gov/data/tcr/AL032021_Claudette.pdf.

Park, M.-S., M.-I. Lee, D. Kim, M. M. Bell, D.-H. Cha, and R. L. Elsberry, 2017: Land-based convection effects on formation of Tropical Cyclone Mekkhala (2008). *Mon. Wea. Rev.*, **145 (4)**, 1315–1337, https://doi.org/10.1175/MWR-D-16-0167.1.

Petersen, W. A., S. A. Rutledge, and R. E. Orville, 1996: Cloud-to-ground lightning observations from TOGA COARE: Selected results and lightning location algorithms. *Monthly Weather Review*, **124 (4)**, 602–620, https://doi.org/10.1175/1520-0493(1996)124<0602:CTGLOF>2.0.CO;2.

Peterson, M., T. E. Light, and D. Mach, 2022: The illumination of thunderclouds by lightning: 1. The extent and altitude of optical lightning sources. *Journal of Geophysical Research: Atmospheres*, **127 (1)**, e2021JD035 579.

Reasor, P. D., M. T. Montgomery, and L. F. Bosart, 2005: Mesoscale observations of the genesis of Hurricane Dolly (1996). *J. Atmos. Sci.*, **62 (9)**, 3151–3171.

Rudlosky, S. D., S. J. Goodman, K. S. Virts, and E. C. Bruning, 2019: Initial Geostationary Lightning Mapper observations. *Geophys. Res. Lett.*, **46 (2)**, 1097–1104, https://doi.org/10.1029/2018GL081052.

Slocum, C. J., M. N. Razin, J. A. Knaff, and J. P. Stow, 2022: Does ERA5 mark a new era for resolving the tropical cyclone environment? *Journal of Climate*, **35 (21)**, 7147–7164, https://doi.org/10.1175/JCLI-D-22-0127.1.

Sokolowsky, G. A., and Coauthors, 2024: tobac v1. 5: Introducing fast 3D tracking, splits and mergers, and other enhancements for identifying and analysing meteorological phenomena. *Geoscientific Model Development*, **17 (13)**, 5309–5330.

Stevenson, S. N., K. L. Corbosiero, M. DeMaria, and J. L. Vigh, 2018: A 10-year survey of tropical cyclone inner-core lightning bursts and their relationship to intensity change. *Wea. Forecasting*, **33 (1)**, 23–36, https://doi.org/10.1175/WAF-D-17-0096.1.

Takahashi, T., 1978: Riming electrification as a charge generation mechanism in thunderstorms. *Journal of Atmospheric Sciences*, **35 (8)**, 1536–1548.

Tang, B. H., and Coauthors, 2020: Recent advances in research on tropical cyclogenesis. *Tropical Cyclone Research and Review*, **9 (2)**, 87–105.

Thiel, K. C., K. M. Calhoun, A. E. Reinhart, and D. R. MacGorman, 2020: GLM and ABI characteristics of severe and convective storms. *Journal of Geophysical Research: Atmospheres*, **125 (17)**, e2020JD032 858, https://doi.org/10.1029/2020JD032858.

Trabing, B. C., K. Hilburn, S. Stevenson, K. D. Musgrave, and M. DeMaria, 2024: Quality control of Geostationary Lightning Mapper observations for tropical cyclone applications. *J. Atmos. Oceanic Technol.*, **41 (9)**, 889–901, https://doi.org/10.1175/JTECH-D-23-0138.1.

Wang, Z., 2018: What is the key feature of convection leading up to tropical cyclone formation? *J. Atmos. Sci.*, **75 (5)**, 1609–1629.

Zawislak, J., and E. J. Zipser, 2014: A multisatellite investigation of the convective properties of developing and nondeveloping tropical disturbances. *Mon. Wea. Rev.*, **142 (12)**, 4624–4645.

Zhang, D., and K. L. Cummins, 2020: Time evolution of satellite-based optical properties in lightning flashes, and its impact on GLM flash detection. *Journal of Geophysical Research: Atmospheres*, **125 (6)**, e2019JD032 024, https://doi.org/https://doi.org/10.1029/2019JD032024.

Zipser, E. J., and C. Gautier, 1978: Mesoscale events within a GATE tropical depression. *Mon. Wea. Rev.*, **106 (6)**, 789–805.